FINAL REPORT

on

FAILURE ANALYSIS OF INCONEL 600® TUBES FROM OTSG A AND B OF THREE MILE ISLAND UNIT-1

to

GPU-NUCLEAR

June 30, 1982

by

Arun K. Agrawal, William N. Stiegelmeyer
Warren E. Berry

BATTELLE
Columbus Laboratories
505 King Avenue
Columbus, Ohio 43201

TABLE OF CONTENTS

LIST OF FIGURES

LIST OF FIGURES (Continued)

LIST OF FIGURES (Continued)

LIST OF FIGURES (Continued)

LIST OF TABLES

LIST OF TABLES (Continued)

FINAL REPORT

on

FAILURE ANALYSIS OF INCONEL 600® TUBES FROM OTSG A AND B OF THREE MILE ISLAND UNIT-1

to

GPU-NUCLEAR

from

BATTELLE
Columbus Laboratories

June 30, 1982

by

Arun K. Agrawal, William N. Stiegelmeyer
Warren E. Berry

INTRODUCTION

Three Mile Island-Unit 1 power plant was brought to hot functional status between August and September of 1981 after a long cold shutdown for about two and a half years. The plant was brought back to cold shutdown status and was then hydrotested in November of 1981. On November 21, 1981 small leaks from primary side to secondary side were detected in tubes of the once-through-steam-generator (OTSG). Subsequently, leaking tubes were identified by bubble test and eddy current examination.

Eddy current examination indicated defects also in some other tubes. As a result, a few tubes with defect indications were removed, along with known leakers, from OTSG-B for determining the nature of the defect(s).

Two tubes from OTSG-B, identified as B-8-25 and B-11-23 were received at BCL on December 28, 1981 for failure analysis. Tube B-11-23

was a known leaker; a quick metallographic examination of the defect in this tube established that the failure was due to intergranular stress-corrosion cracking (IGSCC), and the IGSCC had initiated on the inside surface of the tube.

While detailed examinations of the two tubes were proceeding, two more shipments of tubes pulled from the OTSG-A were received at BCL for similar examinations. The first shipment from GPU-Nuclear was received at BCL on January 21, 1981; it contained four tubes with identifications A-71-126, A-88-11, A-112-5 and A-146-8. The second shipment contained two tubes with identifications A-23-93 and A-146-6; this shipment was received on January 27, 1982.

All the tubes shipped to BCL were from the upper tubesheet (UTS) region of OTSGs A and B. Tubes B-8-25, B-11-23, A-23-93, A-88-11, A-112-5, A-146-6 and A-146-8 were "short-pulls", i.e., these were approximately 12 to 12.5 inch long segments cut from the upper tubesheet crevice region.

Only one tube, A-71-126, was a "long-pull", i.e., it included sections of the tube from beyond the UTS crevice. This tube was received in five segments, labled A-71-126(1) for the top section and then sequentially up to A-71-126(5) for the bottom-most section. The total combined length of all the five segments was 68 inches.

This report contains the results of various examinations conducted on the above tubes at Battelle. Probable cause of the attack also has been identified

APPROACH

The detailed failure analysis program for TMI-Unit-1 tubes was developed in close consultation with GPU-Nuclear personnel. There were two main objectives in this program: 1) to identify and characterize the nature of defect(s) in various tubes, and 2) to determine the probable cause(s) of attack which produced the defect(s). A third objective of the program was to identify, based upon the plant history data provided by GPU-N, the environmental condition(s) which may have been responsible for the attack.

The broad base failure analysis program consisted of the following examinations and tests:

Nondestructive examination (NDE)
Metallography and Microstructural examinations
Microanalytical surface examination and
Physical tests.

The NDE included visual and photographic inspection, X-ray radiography and eddy currect (EC) inspection. The EC inspection used two different types of probes: a standard probe (i.e., differential probe) and an absolute probe (i.e., pencil probe). The pencil probe was used to specifically inspect the roll transition region, i.e., the area between the rolled section and the unrolled section of a tube.

Radiography was used to locate defects that produced sufficient discontinuity in the tube wall for a relatively easy penetration of X-rays. For example, the technique was very helpful in locating the through-wall, but not easily visible crack in tube B-11-23.

There were a few tubes which had obvious "lip-cracks", i.e., a broken off wall within 0.25 inch of the top end. These "lip-cracks" were photographed for documentation purposes.

Metallographic and microstructural examination involved examining longitudinal and transverse cross section of specimens removed from different locations of various tubes. Specimens were examined in the as-polished condition and some after etching with nital or phosphoric acid. Some specimens were examined in the scanning electron microscope (SEM). One fracture surface was examined with the transmission electronmicroscope (TEM).

In order to determine the nature of corrodent responsible for the attack, surface compositions of several tube specimens were investigated. Both the inside diameter (ID) surface and the attacked area, e.g., fracture surface were analyzed. Techniques used in microanalysis of surfaces were energy dispersive X-ray analysis (EDAX), Auger electron spectroscopy (AES), electron spectroscopy for chemical analysis (ESCA), secondary ion mass

spectroscopy (SIMS) and electron microprobe analysis (EPMA) for X-ray images of elements. X-ray differaction (XRD) also was used for corrosion product identification.

Bulk composition of tube material also was determined. X-ray fluorescence and other standard methods were used for this purpose.

Physical tests of tubes or tube material included, 1) tension test, 2) wall thickness measurement and 3) microhardness measurement using Knoop diamond pyramid tester.

The susceptibility of a few tubes to intergranular attack (IGA) by polythionic acid was investigated using the electrochemical potentiokinetic reactivation technique (EPR).

In support of the failure analysis program, five wipe samples from OTSGs A and B were also supplied by GPU-Nuclear. These were analyzed using γ-ray isotopic analysis for the determination of active isotopes present in OTSGs.

3.0 RESULTS OF NONDESTRUCTIVE EXAMINATION

3.1 Introduction

Tube segments from GPU-Nuclear were received packaged in 40 gallon drums. After opening the packages, each tube segment was subjected to four different nondestructive examinations (NDEs). The NDEs performed were:

(1) Radiation level check
(2) Visual and photographic
(3) X-ray radiographic
(4) Eddy current inspection

3.2 Radiation Level Check

The radiation level of each tube segment was checked to establish safe working conditions. The radiation level at contact for different tubes ranged between 20 mR/hr and 40 mR/hr. The above radiation levels were considered low, nonetheless, appropriate safety precautions were still required when working with these tubes, in order to protect both personnel and work facilities from radioactive contamination.

3.3 Visual and Photographic

3.3.1 Results. Initial visual inspection of tubes (segments) showed no obvious defects in the form of a crack or a pit on the OD surface, except for the dryout water marks and some scratch marks; the latter probably were from the tube cutting and pulling operations. Tube ends in a few cases, however, were more ragged than in others, this again was considered to be a result of tube removal operations.

Tube defects in the form of lip-cracks were observed at the upper (top) end of tubes A-88-11, A-112-5 and A-146-8. The lip-crack in each case was associated with the 0° orientation slot cut in the tube.

Following the initial visual inspection, each tube was photographed in four different positions, i.e., 0°, 90°, 180° and 270°. An inch scale also was photograghed along side of each tube to show its length.

Photographs of tube B-8-25 are shown in Figure 1; water marks are visible along the whole length of the tube and in all four positions, i.e., 0°, 90°, 180° and 270°. A closeup view of the dryout mark at 90° is shown in Figure 2.

Photographs of tube B-11-23 are shown in Figure 3; water marks are visible along the whole length of the tube and in all four positions. The 270° quadrant, however, was relatively cleaner than the other three quadrants.

Photographs of tube A-23-93 are shown in Figure 4 with water marks visible along the whole length of the tube and in all four positions. A closeup view of the top end at 90° position is shown in Figure 5. Some vertical scratch marks are clearly visible in the rolled section (0-1.0 in.) of the tube. The end of the rolled section is indicated by the circumferential white ring at 1.0 inch.

Tube A-71-126 was a long-pull and it was received at BCL in five segments. These segments were marked 1 to 5, in the order in which they were removed from the OTSG, i.e., 1 for the top segment and 5 for the bottom most. Photographs of segments one through five are shown in Figures 6 through 10, respectively. Water marks on tube A-71-126 were less extensive and dense, particularly those on lower segments, than those observed on the previous three tubes. However, all four quadrants of the five segments of tube A-71-126 showed some water spots. No particular quadrant was free of water spots.

Figure 7 for tube A-71-126 segment 2 shows circumferential shiny ring pattern over most of the tube surface, particularly in the first 7 inches of the segment. These rings are obviously from the mechanical operation of tube removal, but such an extensive marking was not observed on any other tubes.

Photographs of tube A-88-11 are shown in Figure 11, water marks on the 0° quadrant are relatively heavier than on the other three quadrants.

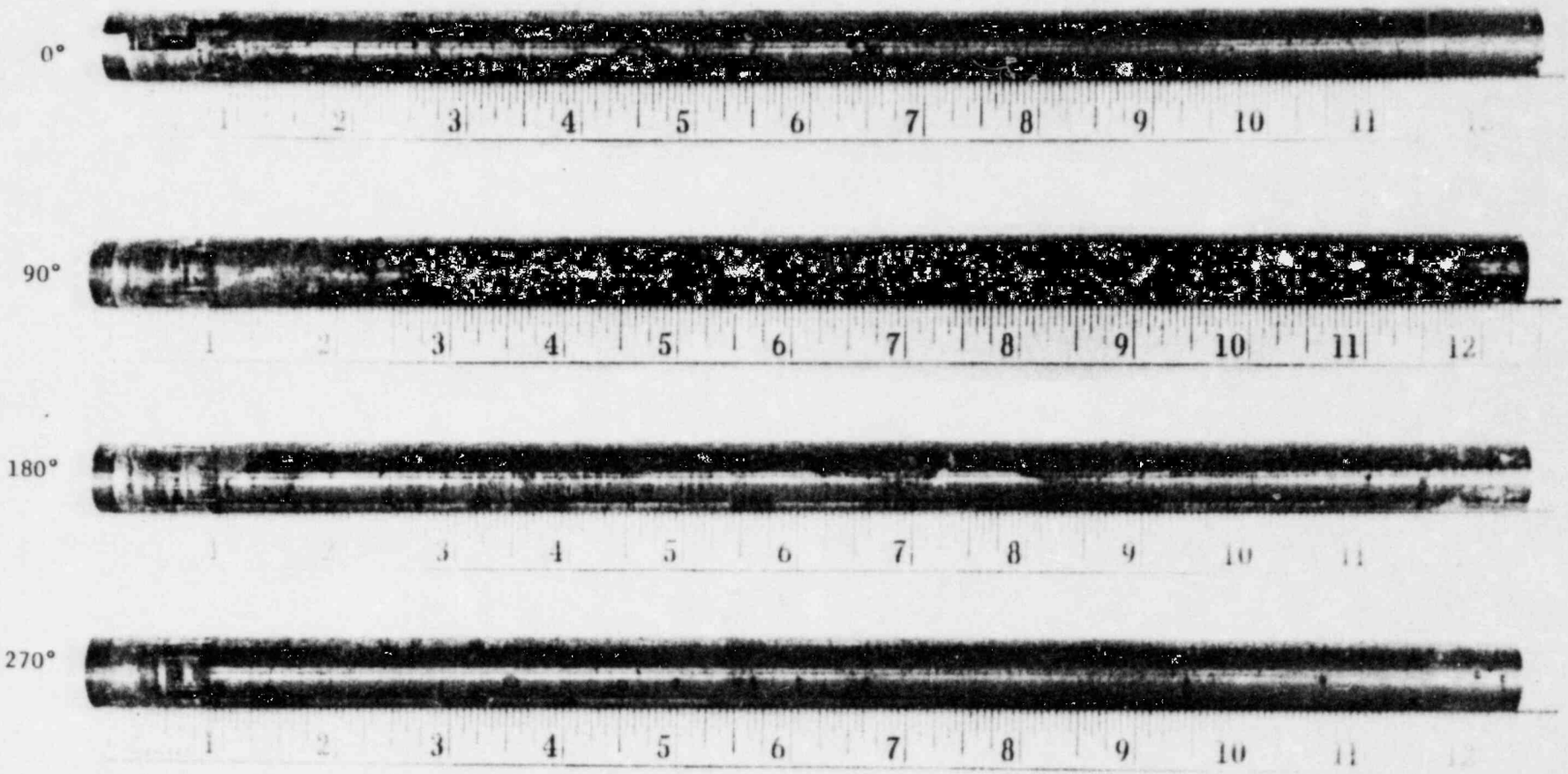

FIGURE 1. APPEARANCE OF AS-RECEIVED TUBE B-8-25 AT 0, 90, 180 AND 270 DEGREE POSITIONS

FIGURE 2. A CLOSEUP VIEW OF THE DRYOUT MARKS ON TUBE B-8-25 AT 90 DEGREE POSITION

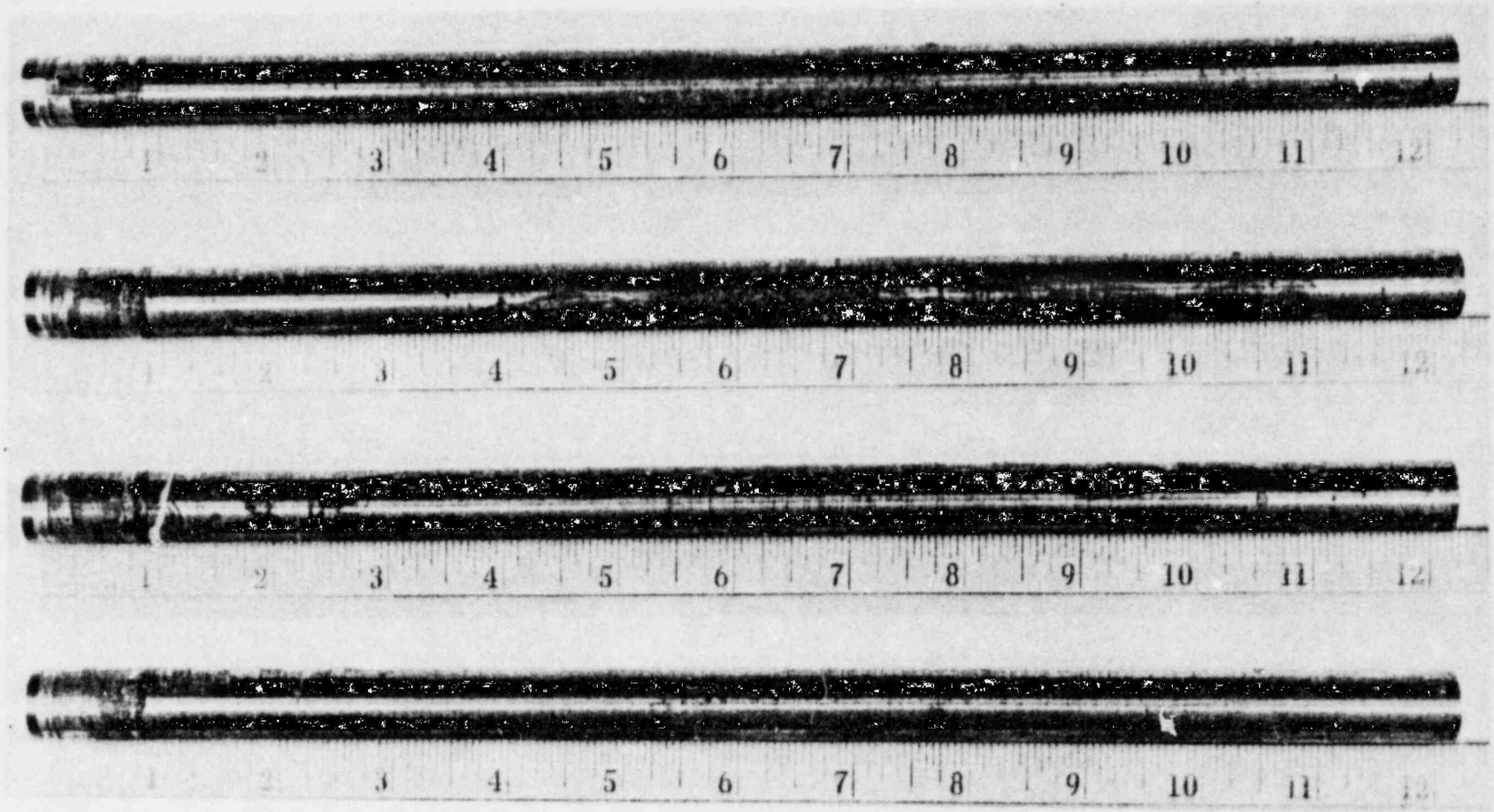

FIGURE 3. APPEARANCE OF AS-RECEIVED TUBE B-11-23 AT 0, 90, 180 AND 270 DEGREE POSITIONS

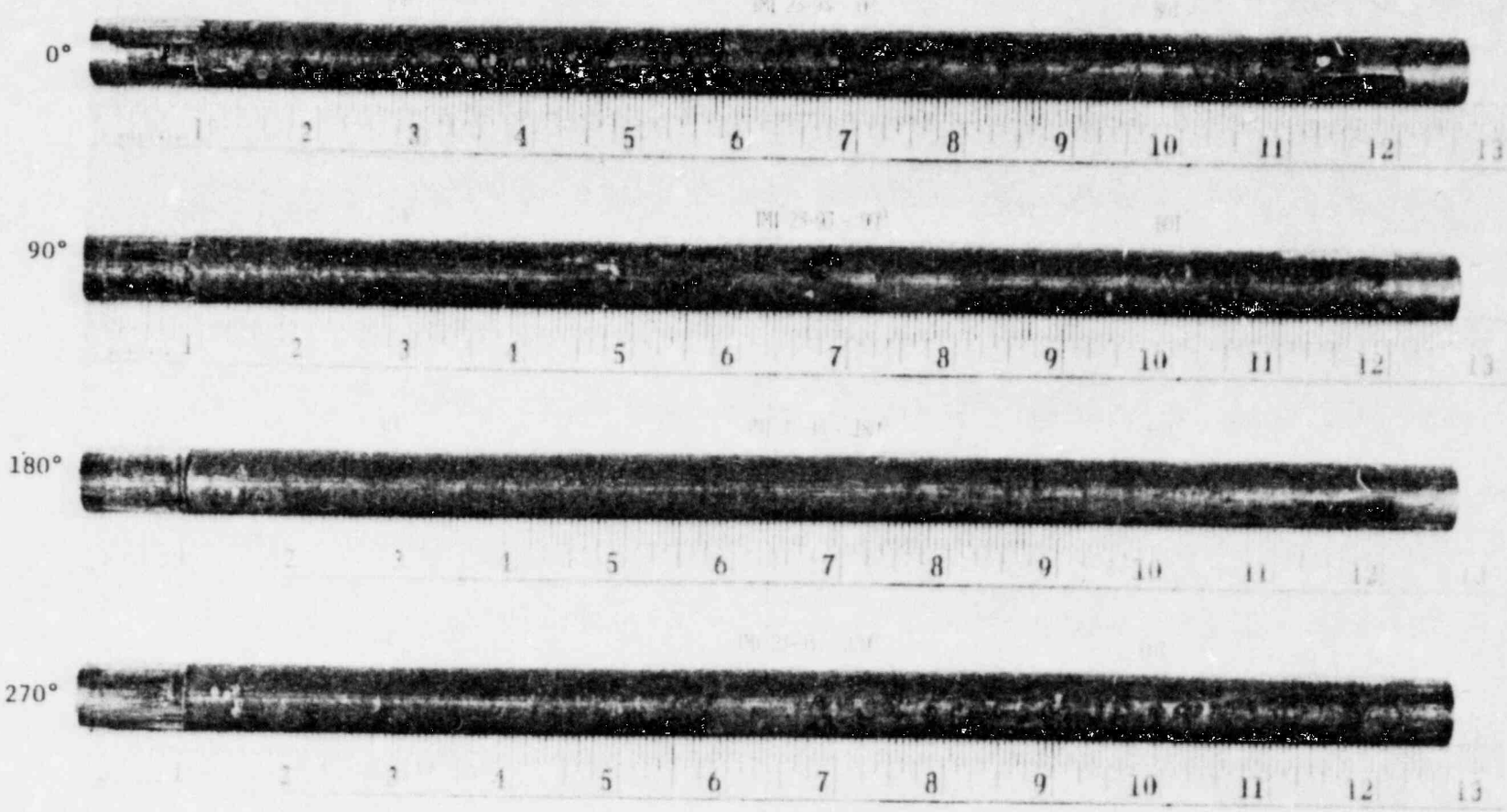

FIGURE 4. APPEARANCE OF AS-RECEIVED TUBE A-23-93 AT 0, 90, 180 AND 270 DEGREE POSITIONS

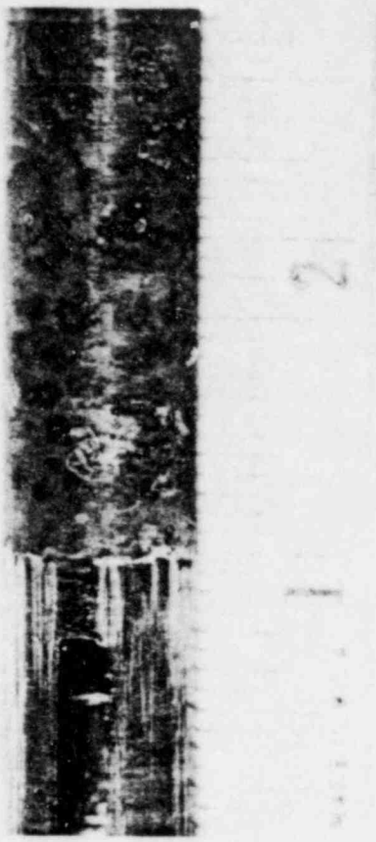

FIGURE 5. A CLOSEUP VIEW OF THE DRYOUT MARKS ON TUBE A-23-93 AT 90 DEGREE POSITION

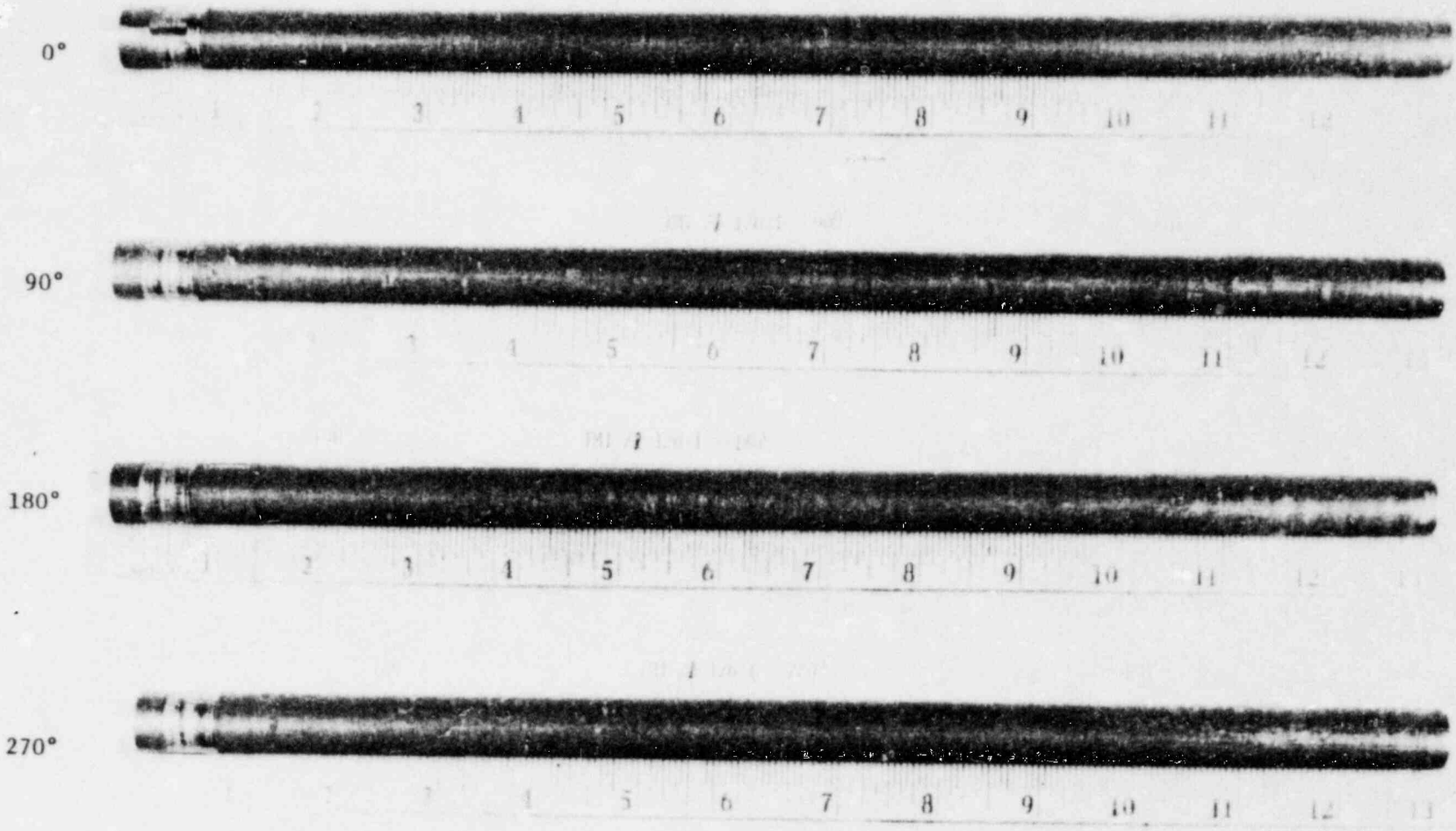

FIGURE 6. APPEARANCE OF AS-RECEIVED TUBE A-71-126 SEGMENT 1 0, 90, 180 AND 270 DEGREE POSITIONS

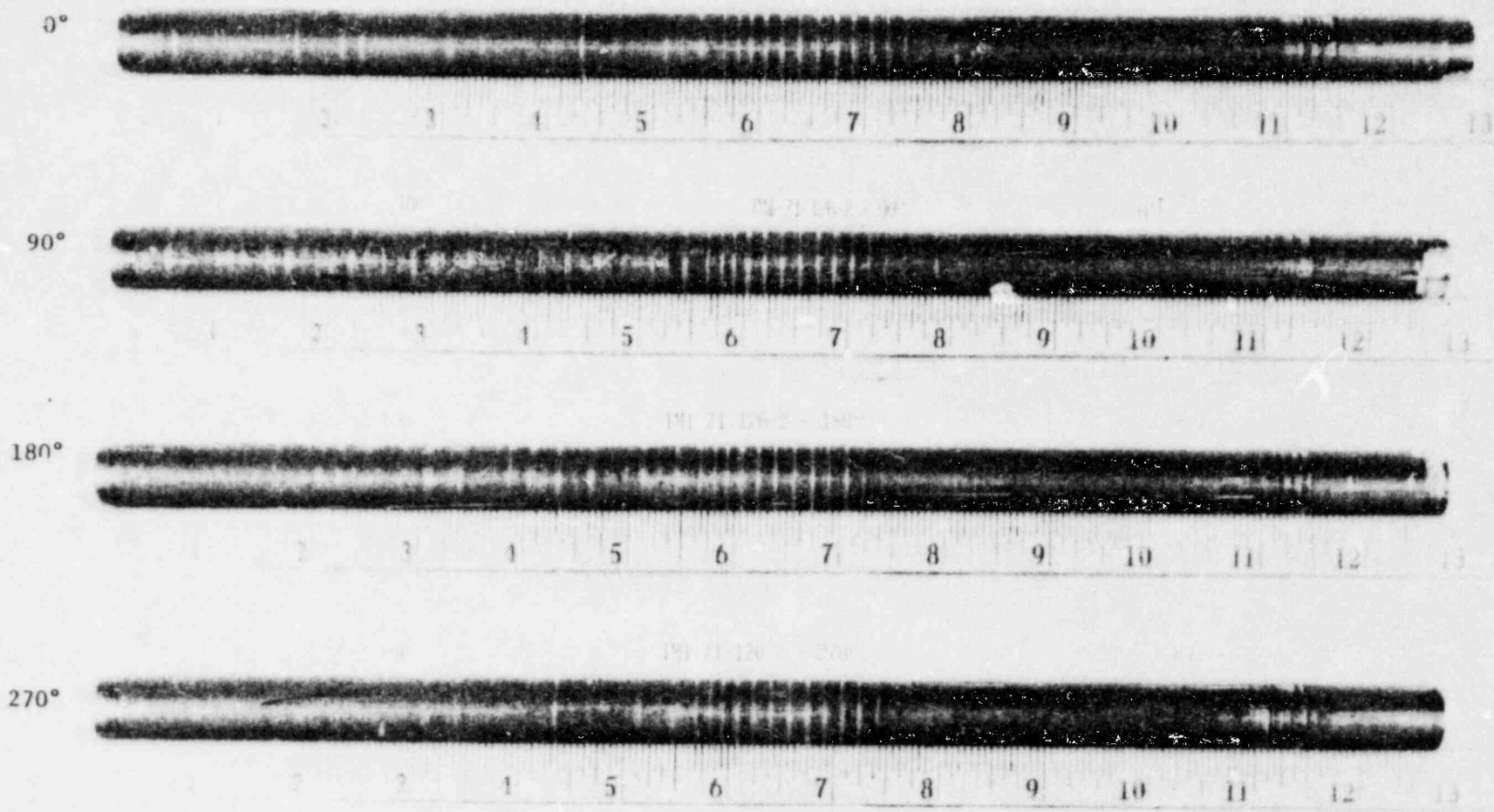

FIGURE 7. APPEARANCE OF AS-RECEIVED TUBE A-71-126 SEGMENT 2 AT 0, 90, 180 AND 270 DEGREE POSITIONS

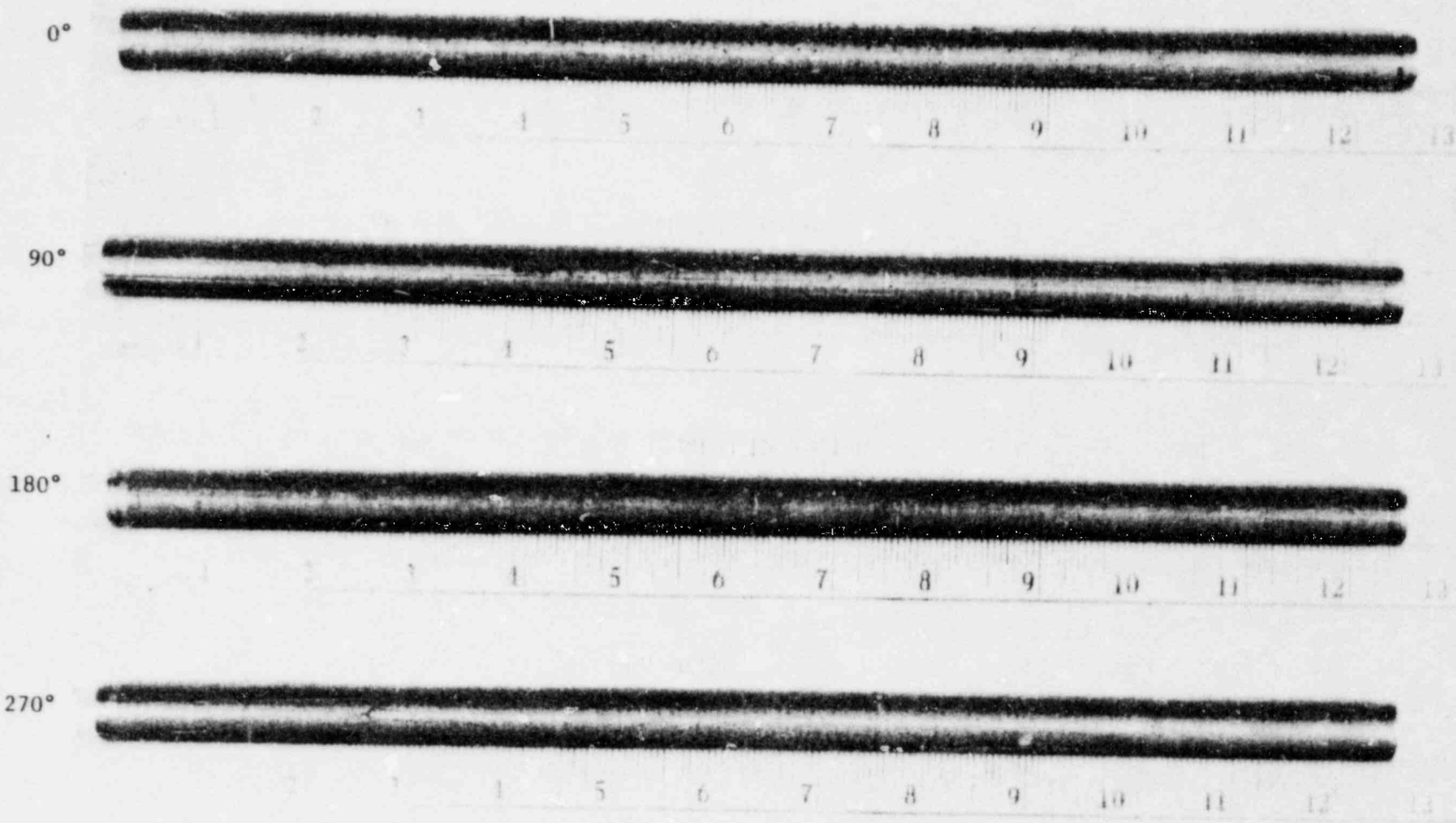

FIGURE 8. APPEARANCE OF AS-RECEIVED TUBE A-71-126 SEGMENT 3 AT 0, 90, 180 AND 270 DEGREE POSITIONS

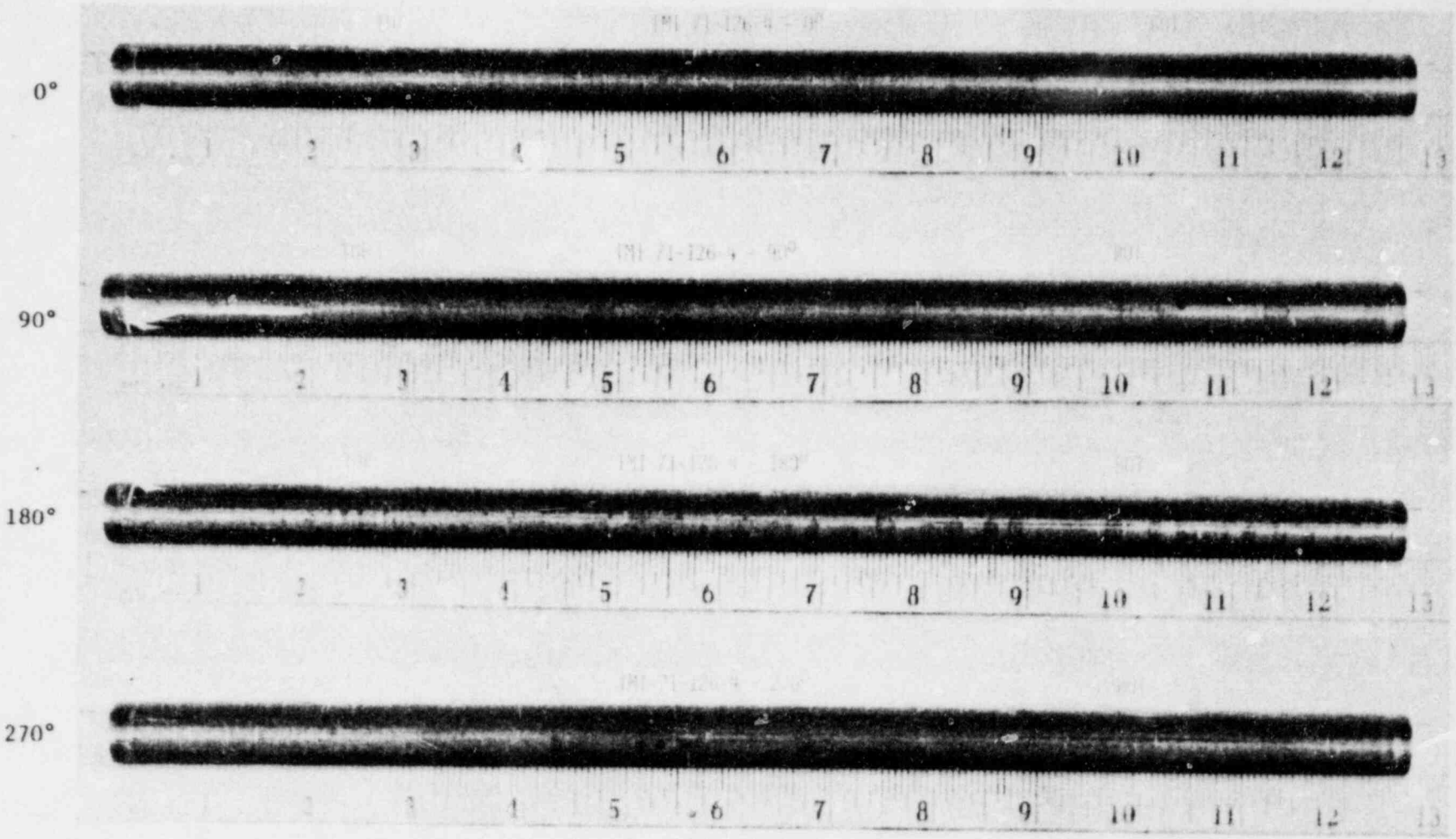

FIGURE 9. APPEARANCE OF AS-RECEIVED TUBE A-71-126 SEGMENT 4 AT 0, 90, 180 AND 270 DEGREE POSITIONS

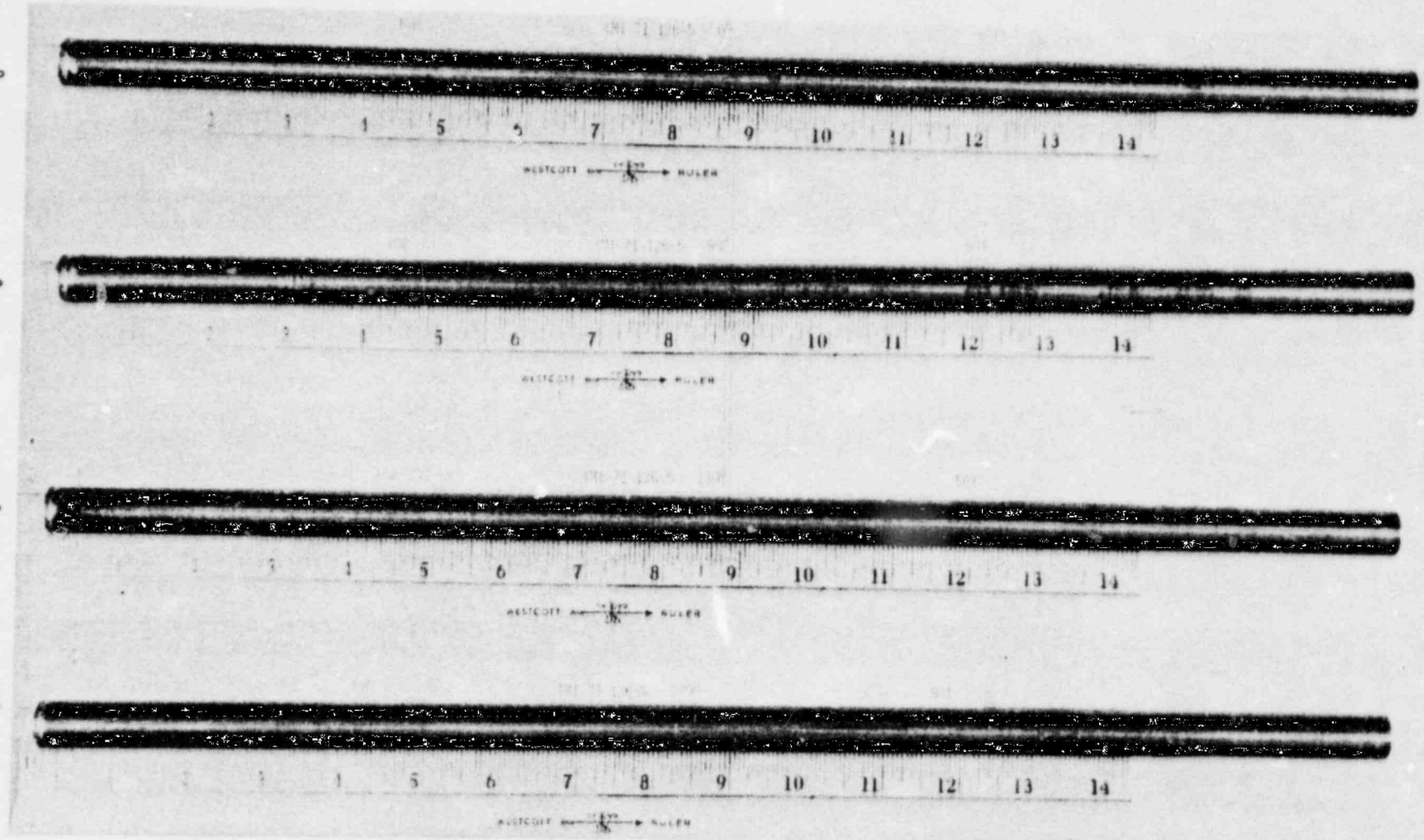

FIGURE 10. APPEARANCE OF AS-RECEIVED TUBE A-71-126 SEGMENT 5 AT 0, 90, 180 AND 270 DEGREE POSITIONS

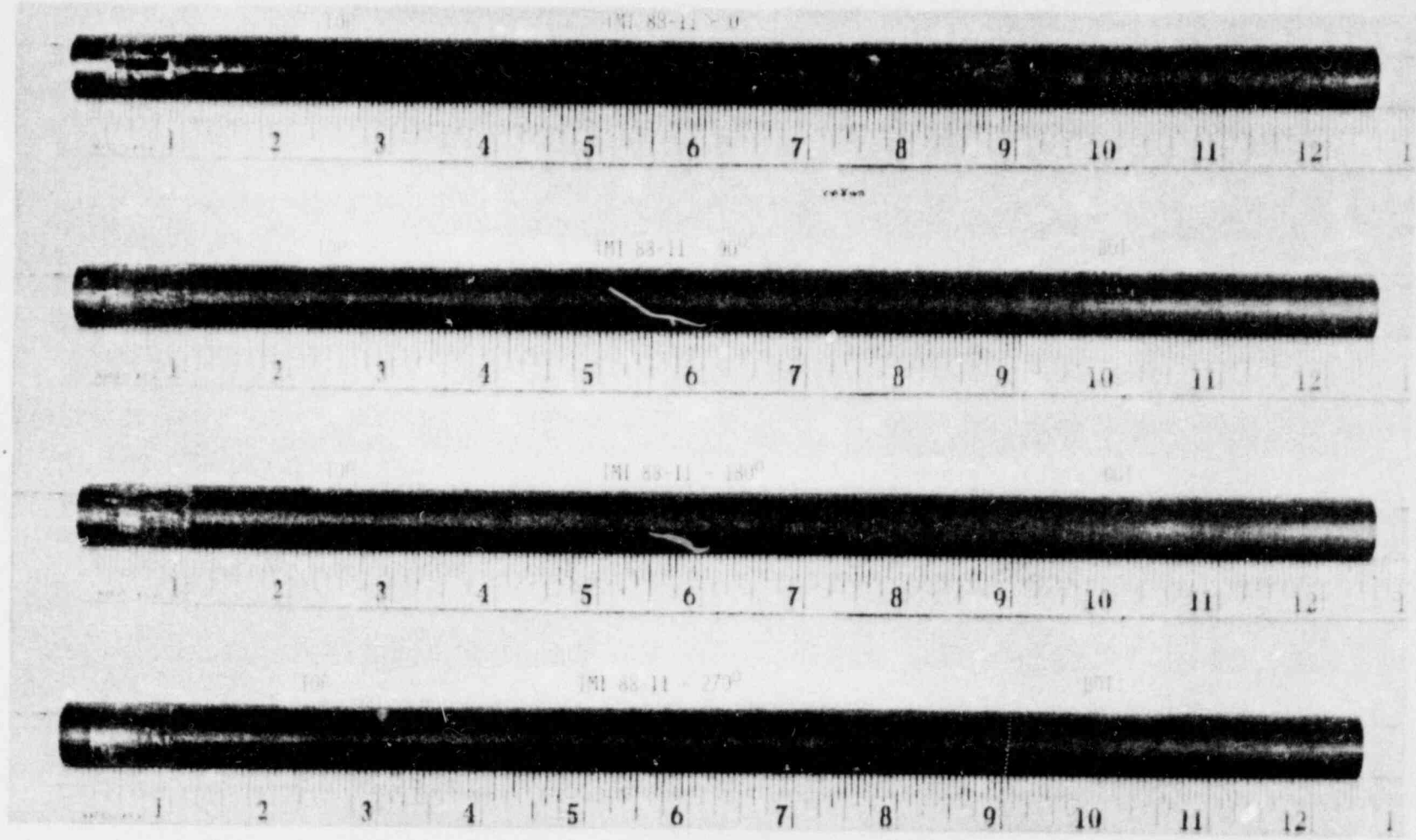

FIGURE 11. APPEARANCE OF AS-RECEIVED TUBE A-88-11 AT 0, 90, 180 AND 270 DEGREE POSITIONS

A closeup view of the dryout deposits in 0° quadrant is shown in Figure 12. The lip-crack, described earlier, can be seen at the slotted end in the 0° photograph.

Photographs of tubes A-112-5, A-146-6 and A-146-8 are shown in Figures 13, 14 and 15 respectively. Dryout water marks are present along the whole length and in all four quadrants of these tubes. Some vertical scratch marks in the rolled section of tubes and circumferential water ring at the end of rolled section are also visible in these photographs. Some scratch marks at other places along the tube length also can be seen in Figures 13 and 14.

In Figure 13 a lip-crack can be seen extending from the slot in tube A-112-5. A similar lip-crack is visible in tube A-146-8 in Figure 15.

3.3.2 Significant Observations. Visual and photographic examinations of the OD surface of tubes are summarized below:

(1) Dryout water marks were present practically on all tubes. These marks were present practically on all four quadrants of each tube.
(2) Vertical scratches were observed on all tubes at various locations, but the scratches were particularly heavy in the rolled section of each tube.
(3) Some shiny circumferential ring patterns were observed on some tubes; the ring patterns were numerous on segment 2 of tube A-71-126 and are probably the result of the tube pulling operation.
(4) Lip-cracks were observed in tubes A-88-11, A-112-5 and A-146-8; the cracks were associated with 0° orientation slot in each case.

3.4 X-ray Radiographic Examination

3.4.1 Results. Each tube segment was radiographed individually in four different positions, at approximately 0°, 90°, 180° and

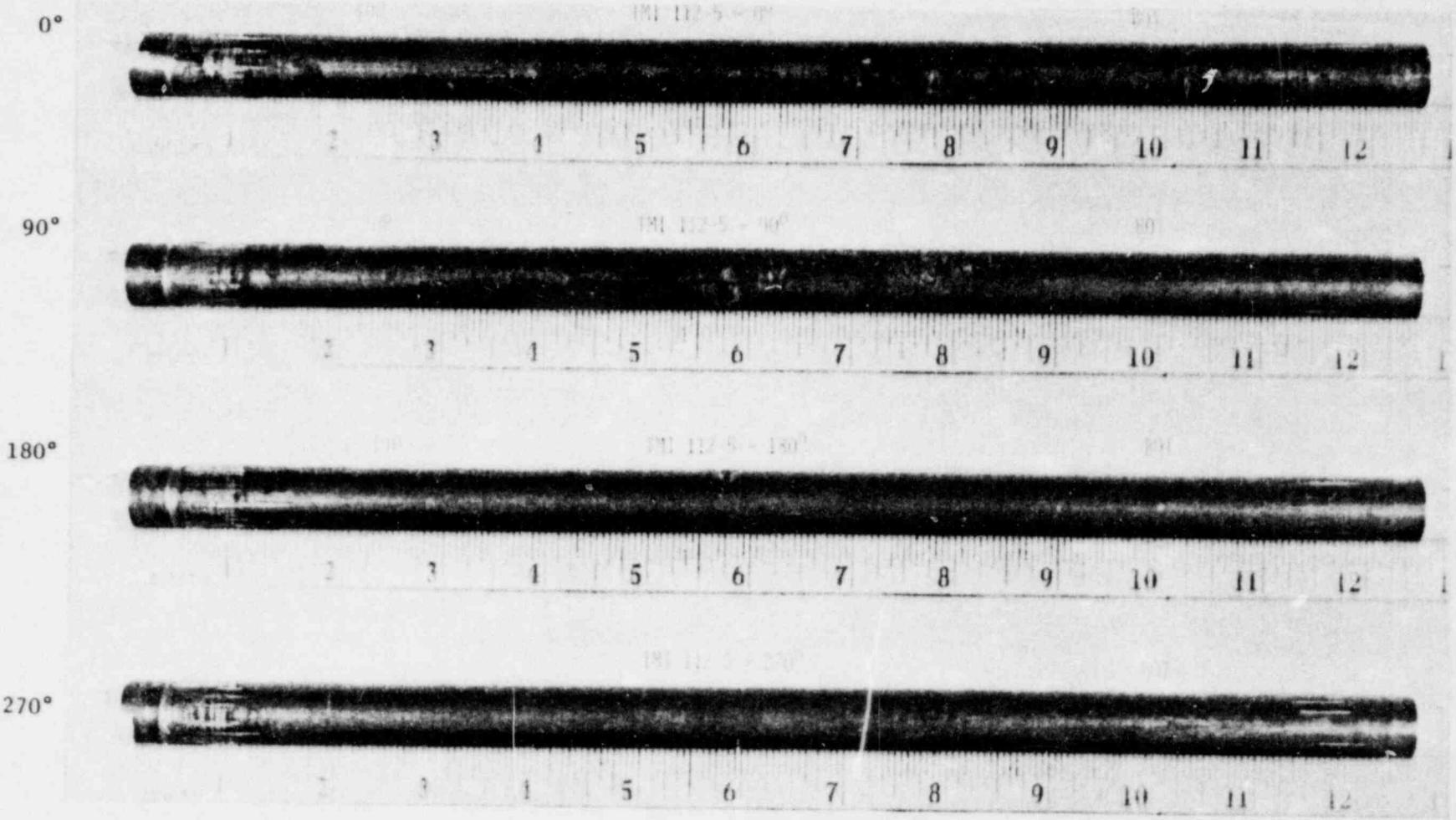

FIGURE 13. APPEARANCE OF AS-RECEIVED TUBE A-112-5 AT 0, 90, 180 AND 270 DEGREE POSITIONS

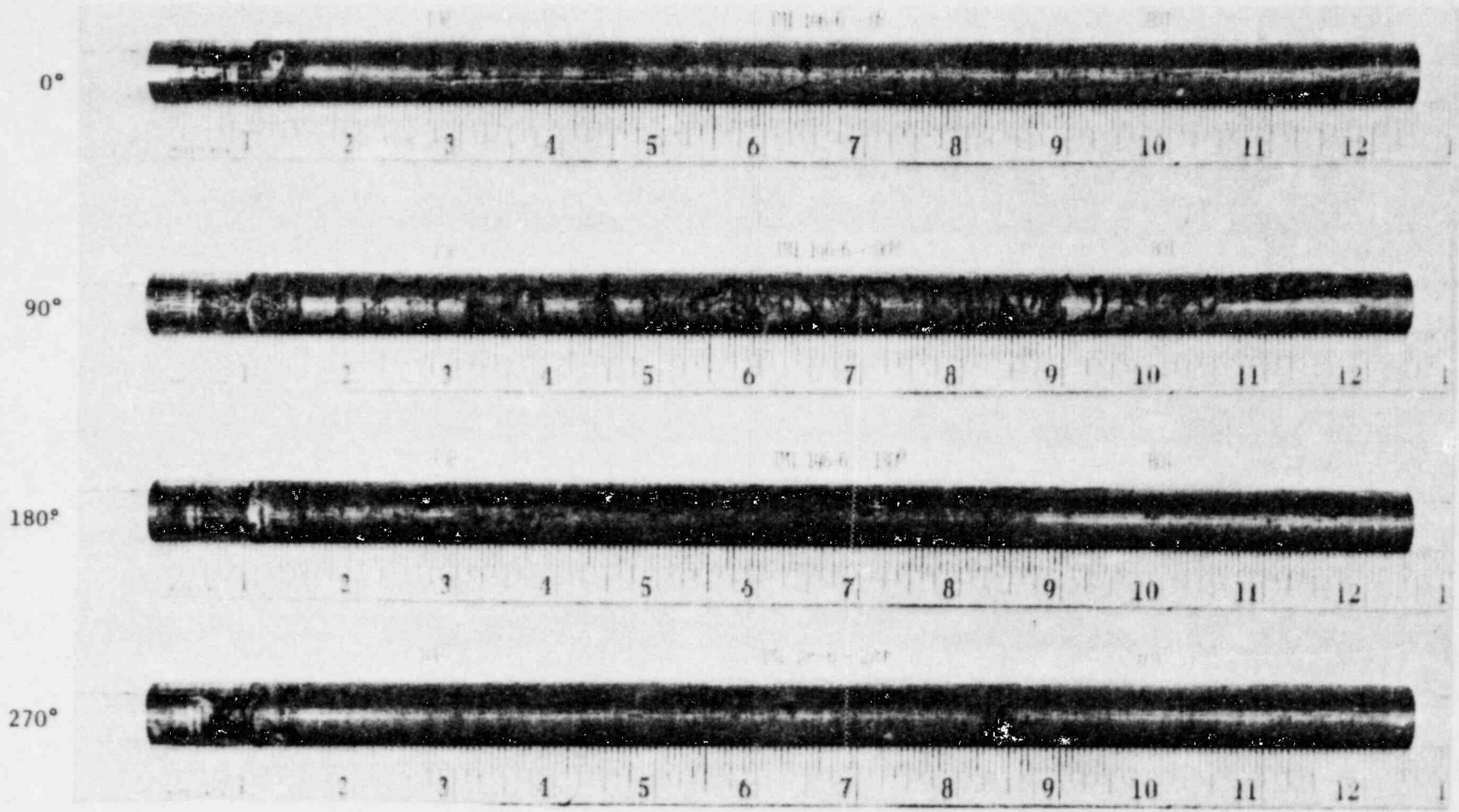

FIGURE 14. APPEARANCE OF AS-RECEIVED TUBE A-146-G AT 0, 90, 180 AND 270 DEGREE POSITIONS

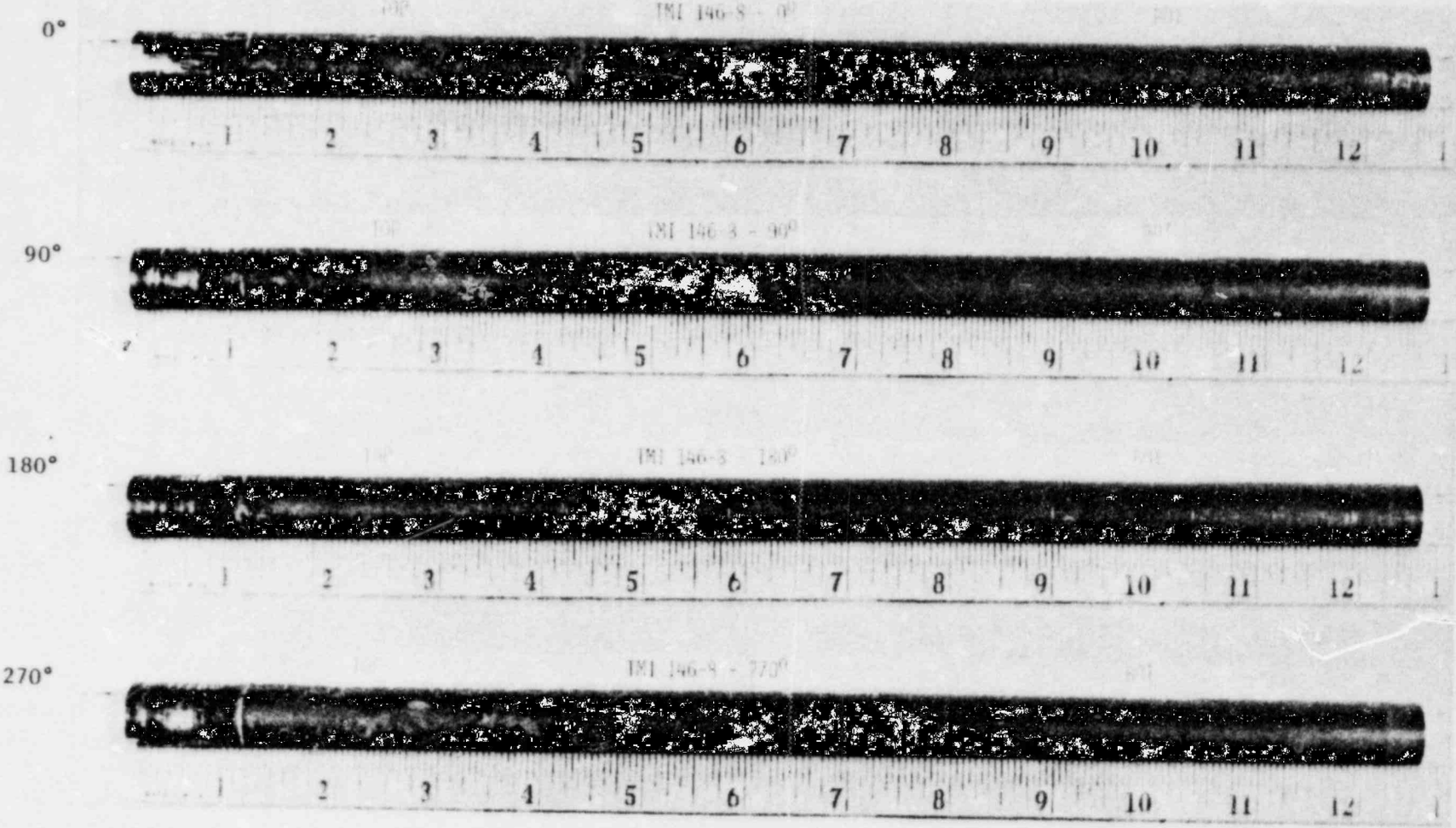

FIGURE 15. APPEARANCE OF AS-RECEIVED TUBE A-146-8 AT 0, 90, 180 AND 270 DEGREE POSITIONS

270°. Then each radiograph was examined over a light viewer to observe changes in light density over the radiograph's surface. In several radiographs, dark hairlines were observed against the light general background. These dark hairlines were considered as indicative of defects (possibly narrow hairline cracks) in the corresponding area on the tube.

The hairlines in practically all cases ran in transverse direction and covered anywhere from 1/10th to 3/4th of the tube diameter. A defect shown by a hairline was classified as a "clear" indication if the hairline was sufficiently dark, otherwise as a "faint" indication. The location of each indication was recorded. All the indications observed on various tubes are listed in Table 1.

No vertical (longitudinal) hairline indications were observed corresponding to the OD surface scratches described earlier in Subsection 3.2. This implies that the scratches were superficial, only surface deposit deep, and did not scar the metal underneath, otherwise indications would have been obtained.

3.4.2 Significant Observations. Results of radiographic examination of various tubes are summarized below:

(1) Defect indications for lip-cracks were obtained in tubes A-23-93, A-88-11, A-112-5 and A-146-8. The indications were faint in tube A-88-11, but clear in the other three.

(2) Defect indications in the vicinity of roll transition area (i.e., location 0.75 to 1.25 inch) were obtained in tubes A-88-11, A-112-5, A-146-6, A-146-8 and B-11-23. The indication was faint in tube A-146-8 but clear in the other four tubes.

(3) There were several clear defect indications in all tube segments examined; including segment 5 of tube A-71-126 which was removed from below the upper tube sheet of OTSG-A.

TABLE 1. DEFECT INDICATIONS IN RADIOGRAPHS OF TUBES FROM TMI-1 STEAM GENERATORS A AND B

Tube Number	Defect Location From the Top of the Tube, Inch							
A-23-93	Lip Crack	2.75-3.25 Faint	12.0 Faint	12.25 Clear				
A-71-126/1	1.75 Clear	12.25 Clear						
A-71-126/2	1.0 Faint	1.75 Faint	6.5 Clear	8.5 Faint	9.75 Clear			
A-71-126/3	4.0 Clear	7.5 Clear	9.0 Clear	9.5 Clear	9.75 Clear	10.0 Clear	12.25 Clear	
A-71-126/4	7.25 Clear	8.5 Faint	9.5 Clear	10.0 Clear	10.75 Clear	11.25 Clear	12.25 Clear	
A-71-126/5	Numerous indications faint to clear along the whole length, 14.5 clear.							
A-88-11	0.25 Faint	1.5 Clear		2.75 Clear	3.5 Clear	7.0 V Shape	9.75 Faint	11.75 Clear
A-112-5	0.25 Lip Crack	1.25 Clear	2.0 Clear	6.0 Clear	11.5 Clear			
A-146-6	0.75 Clear	1.0 Clear	3.25-4.0 Clear	4.25 Clear	4.75 Clear	5.25 Faint	6.0 Clear	6.5 Clear
A-146-8	Lip Crack	0.25 Clear	4.0 Faint	4.0 Faint	4.25 Faint	6.75 Faint	8.5 Faint	
B-8-25	10.25 Faint	11.5 Faint						
B-11-23	1.0 Faint	1.25 Clear	1.5 Clear	2.5 Clear				

3.5 Eddy Current Examination

3.5.1 Results. Two types of eddy current (EC) probes were used in the examination of each tube segment. These were the differential or standard probe (Model No. A520LC) and the pencil probe (also known as the absolute probe). Both probes were obtained from ZETEC Corporation of Washington. An Eddy Scope Model EM 3300 from Automation Industries was used for displaying the signals, which were then recorded with a Polaroid camera. Test frequencies with the differential and pencil probes were 400 kHz and 350 kHz, respectively. The gain in the Eddy Scope was set such that a 100 percent through-wall defect in the ASME Section 11 standard produced a signal which covered one-third the width of the scope screen. The differential probe was calibrated using an ASME Section 11 standard. No calibration was done for the pencil probe.

Results of the EC examination of various tubes are listed in Table 2. The location of each defect indication is given with respect to the top of the tube examined. The circumferential position of a defect is indicated by degrees, following the standard practice (W-axis as 0°) recommended by GPU-Nuclear.

3.5.2 Significant Observations. The results of EC examination are summarized below:

(1) Defect indications in the roll transition region were obtained in tubes B-8-25, A-88-11, A-112-5 and A-146-6.

(2) Defect indications were obtained in all tube segments, including those from the long-pull from below the upper tube sheet crevice region. Location of all indications from various tubes are listed in Table 2.

(3) Some defects indicated by the differential probe were not confirmed by the pencil probe, and vice versa. However, in most cases indication of one probe was confirmed by the other.

TABLE 2. RESULTS OF EC EXAMINATION OF TUBES FROM TMI-1 STEAM GENERATORS A AND B USING DIFFERENTIAL AND PENCIL PROBES

Tube Number	Defect Location* DP in.	Defect Location* PP in, degree	Comment	Note
B-8-25		1.25, 90-180	Large Signal	Bracing roll transition
		1.50, 320	Large Signal	
		2.75, 180	Large Signal	
	3.0		∿90% Wall	
	3.5		∿90% Wall	
	4.0		Surface Defect	
	4.5		Small Signal	
		4.5, 180	Large Signal	
	5.0		Small Signal	
		4.75, 110	Large Signal	
		5.0, 90	Large Signal	
		5.25, 110	Large Signal	
	5.75		Surface Defect	
	6.0		Surface Defect	
		6.75, 90	Large Signal	
		7.75, 60	Large Signal	
		9.25, 340	Small Signal	
	9.25		Surface Defect	
	9.75		Surface Defect	

TABLE 2. (Continued)

Tube Number	Defect Location* DP in.	Defect Location* PP in, degree	Comment	Note
B-11-23		0.25, 25	Large Signal	Tube Stub (2.0 in) was examined after cross sectioning the tube. No indication in roll transition region.
		0.75, 180	Large Signal	
		1.0, 300	Large Signal	
	10.25		Small Signal	Remainder of the tube (long piece) after removing the thru-wall crack.
A-23-93	1.75		Small Signal	
		1.75, 20-140	Large Signal	
	2.5		~80% Wall	
		2.5, 20-140	Large Signal	
A-71-126		2.75, ~0	Small Signal	
	3.0		Small Signal	
A-71-126	14.25		Possibly O.D.	Ends flared to allow probes
	24.25		Possibly O.D.	
A-71-126	33.25		Small Signal	Ends flared to allow probes
		33.25	Small Signal	
	36.75		Possibly O.D.	
A-71-126	49.25		Possibly O.D.	Ends flared to allow probes
A-71-126	52.75		<20% Wall	
		54.25, ~0	Small Signal	

TABLE 2. (Continued)

Tube Number	Defect Location* DP in.	Defect Location* PP in, degrees	Comment	Note
A-88-11		1.25, 270	Large Signal	Bracing roll transition
		5.0, 90	Large Signal	
	5.0		∿100% Wall	
A-112-5		1.25, 270	Small Signal	Bracing roll transition
		3.25, 270	Large Signal	
	3.5		90% Wall	
		5.25, 270	Large Signal	
	6.25		90% Wall	
	6.25		90% Wall	
		6.50, 270	Large Signal	
	8.0		80% Wall	
		8.0, 270	Large Signal	
A-146-6		1.25, 5-260	Large Signal	Bracing roll transition
	4.0		Possibly O.D.	
	8.25		∿70% Wall	
		8.25, 5-260	Large Signal	
	10.25		∿70% Wall	
		10.25, 180-290	Large Signal	

TABLE 2. (Continued)

Tube Number	Defect Location* DP in.	PP in, degrees	Comment	Note
A-146-8	2.0		Medium Signal	
		2.0, 0-270	Medium Signal	
	3.75		~90% Wall	
		3.5, 0	Large Signal	
	6.0		~90% Wall	
		6.0, 350	Large Signal	

* Defect Location refers to the top end of each tube as 0.0 inch and degrees are referenced with respect to W-axis as 0°.

4.0 RESULTS OF OTHER EXAMINATIONS

4.1 Tube B-8-25

Short-pull tube B-8-25 was examined using the following techniques:

(1) Visual examination of U-bend slices
(2) Visual examination of ID surface
(3) Metallographic examination
(4) SEM (Scanning electron microscope) and EDAX (energy dispersive X-ray analysis) examinations of fracture face
(5) AES and ESCA examinations of fracture surface film.

Examination results for tube B-8-25 are summarized in Table 3. Also given in Table 3 are: a) the identification number of each specimen removed from the tube for examination; b) location of each specimen with respect to the top end* and 0° axis of the tube; c) type of any defect indication from NDEs, and d) type of examination performed on each specimen. Details of the examination results are given below.

Top end (specimen A) of tube B-8-25 containing the roll-transition area was slit into eight longitudinal slices. This section had an EC indication at 1.25 inch location. Photographs of these slices (specimens A1-A8) are shown in Figure 16. Specimen A4 broke into two pieces during slitting, and specimen A3 also showed a through-wall crack in handling. Specimens A2, A5 and A6 were bent into U-shape with ID in tension, all three specimens showed cracks with ~90 percent wall penetration. The cracks in specimens A2 through A6 were located at 1.25 inch and spanned from 45° to 270°.

Photomicrographs of the cross section of bent specimen A2 is shown in Figure 17. A crack with 90 percent wall penetration is clearly visible in Figure 17. The crack origin is at the ID surface of the tube.

---

* All locations given herein and after use top of the as-received tube as 0.0 inch reference, with inch fractions converted to nearest 0.25 inch.

TABLE 3. EXAMINATION RESULTS OF TUBE B8-25

Specimen Number	Location		Type of Indication	Examination	Result/Comment
	Inches	Degrees			
A (A1-A8)	0-2.25		EC 1.25	Slit and Bend	No Crack at 0-0.75
A1	0-2.25	0-45		OD Tension, Visual	No Crack
A2	0-2.25	45-90		ID Tension, Met. μ Structure	1.25 IGC, 90% Wall
A3	0-2.25	90-135		SEM/EDAX AES/ESCA	1.25 IGC, 100% Wall; S 1.9% Fission Products and S (0.4%), Be (7.2%), Ag (0.3%) Sulfide
A4	0-2.25	135-180		SEM (top) TEM (bottom)	1.25 IGC, 100% Wall No Striations
A5	0-2.25	180-225		ID Tension, Visual	1.25 IGC, 90% Wall
A6	0-2.25	225-270		ID Tension, SEM/EDAX	1.25 IGC, 90% Wall, S 5.3% Near ID
A7	0-2.25	270-315		OD Tension, SEM	No Crack
A8	0-2.25	315-360		OD Tension, Visual	No Crack
B	2.25-3.25	0-180	EC 3.0, Visual	Crack AES/ESCA	High C (>50 a/o), $S^{=}$ (~1 a/o), Cl (<1 a/o), B (~3 a/o) No $SO_4^{=}$
C1	3.25-12.0	0-180	EC Several Places	ID Visual	Tree Decoration
C2	2.25-12.0	180-360	EC Several Places	ID Visual	Tree Decoration, Crack Appearance at 3.0, 3.5, 4.5

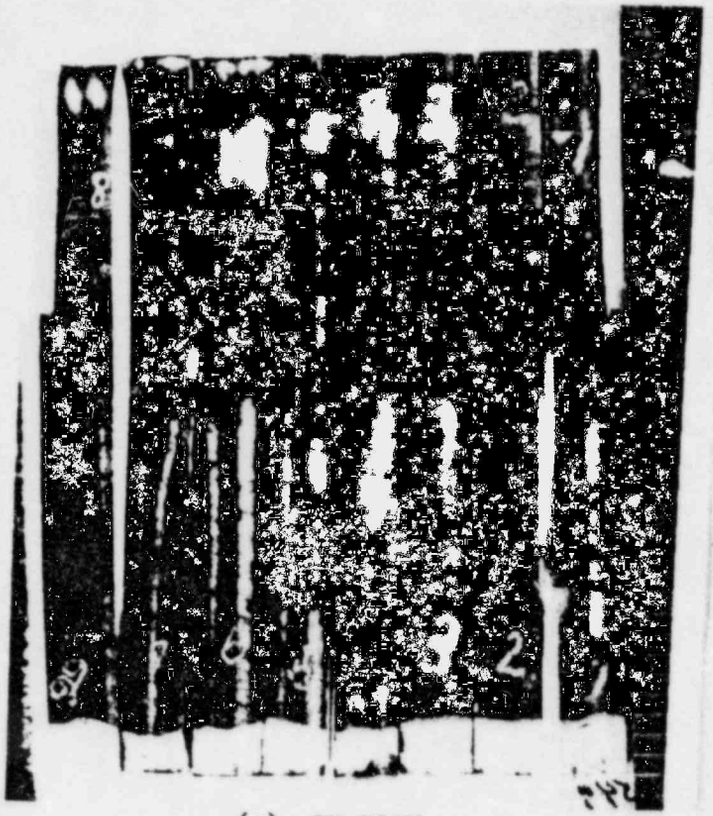

(a) OD VIEW

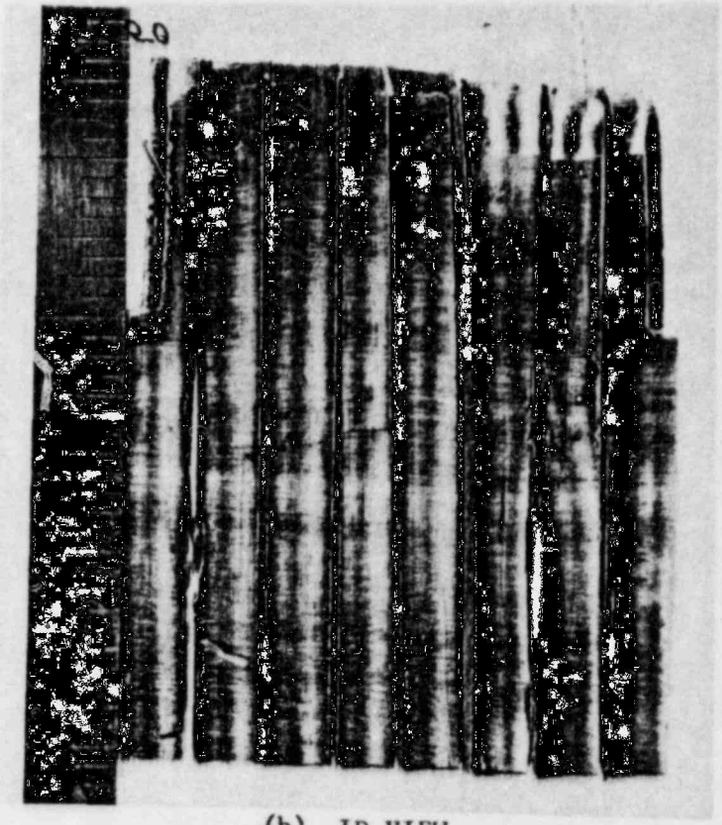

(b) ID VIEW

FIGURE 16. PHOTOGRAPH OF AS-CUT SLICES A1 THROUGH A8 FROM TUBE B-8-25

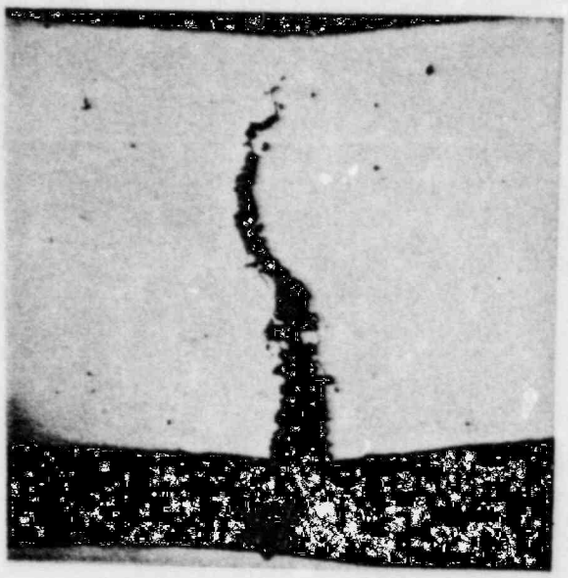

60X

(a) MAIN CRACK

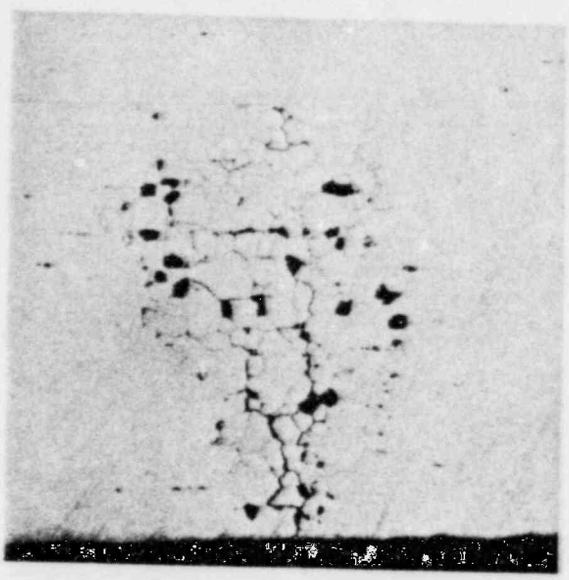

120X

(b) INTERGRANULAR ATTACK

FIGURE 17. PHOTOMICROGRAPHS OF THE CROSS-SECTION OF BENT SPECIMEN A2 FROM TUBE B-8-25

A second IG penetration on the ID surface ∿40 mils above the main crack was also observed, Figure 17b. This IGA penetration is ∿50 percent through wall and the spread at the mid-wall is about 10 grains. SEM photographs of the fractured surface of specimen A6 are shown in Figure 18. The crack is completely intergranular and the wall penetration is >90 percent. Cavities visible on the fractured surface in the mid-wall region indicate that the intergranular penetration was not limited to the transverse direction, but that some penetration also occurred in the longitudinal direction.

The fractured surface of specimen A6, at high magnification showed fluffy deposits on the grain faces, Figure 18. The EDAX analysis of the fractured surface indicated the presence of sulfur. The concentration of S on the surface ranged from 0.4 to 5.3 percent (as relative X-ray intensity ∿ atomic percent), depending upon the area analyzed. Table 4 lists the EDAX results.

The fracture surface of the broken specimen A4 was descaled and then replicated for TEM examination. TEM photomicrographs of the replica are shown in Figure 19. No fatigue striations were observed on the grain facets. This indicates that the failure of the tube was not due to corrosion fatigue but probably was the result of intergranular stress-corrosion cracking (IGC).

Specimens A1, A7 and A8 were bent with OD in tension. None of these showed any crack on the OD or ID surface. Specimen A7 when examined with SEM showed only minor surface tears at the U-bend apex, but no deep cracks, Figure 20.

The crack in specimen A at 1.25 inch was circumferential and limited to specimens A2 to A6 which covered 45° to 270° of the tube.

Specimen A3 was used for AES and ESCA analyses. The surface of A3 that was analyzed contained intergranularly cracked area (∿ 80 percent of surface) and freshly fractured area (∿20 percent of surface); the latter was produced from the mechanical removal of the uncracked ligament from the specimen.

The AES/ESCA instrument used in surface analyses was a Leybold-Heraeus LHS 10 System. The analytical chamber of the instrument operated

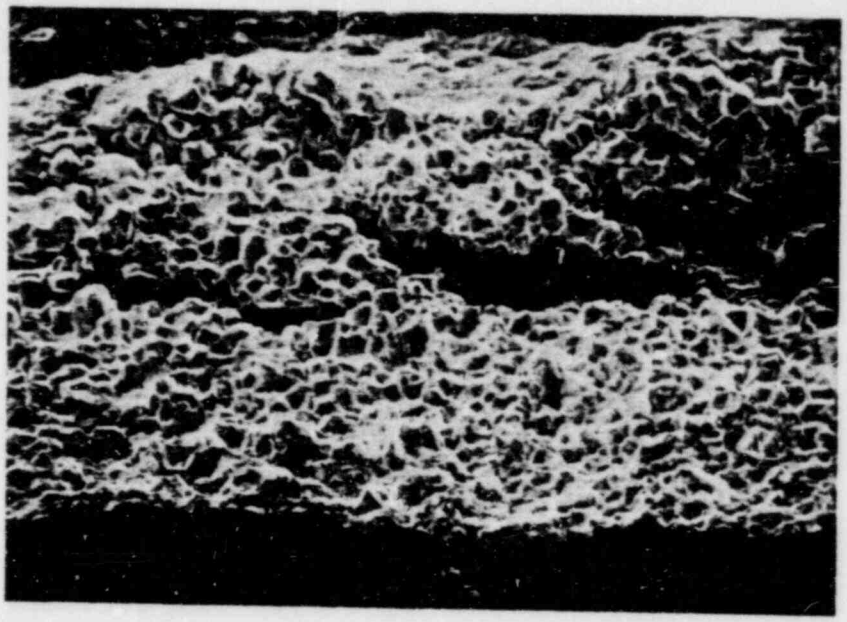

120X

(a) OVERALL VIEW

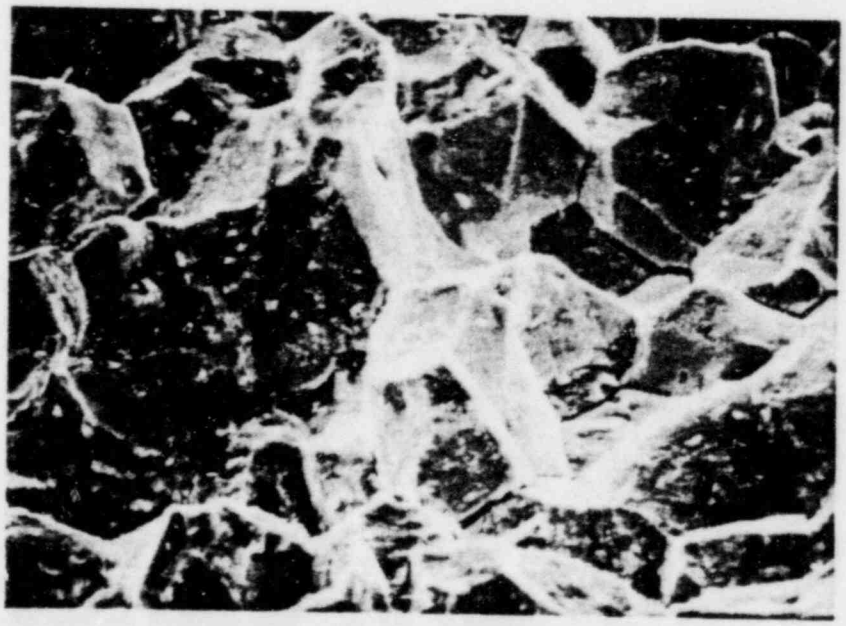

900X

(b) FLUFFY DEPOSITS

FIGURE 18. SEM PHOTOGRAPHS OF THE FRACTURED SURFACE OF SPECIMEN A6 FROM TUBE B-8-25

TABLE 4. EDAX ANALYSIS OF FRACTURE SURFACE OF SPECIMEN A6 FROM TUBE B-8-25

Relative X-Ray Intensity

	Tear Area In Remaining Ligament	Fracture Close To Tear	Fracture Center	Fracture Close To I.D.
Cr	16.5	17.1	18.3	18.0
Fe	10.1	7.2	7.3	4.0
Ni	73.4	74.9	73.4	72.6
S	-	0.7	0.4	5.3

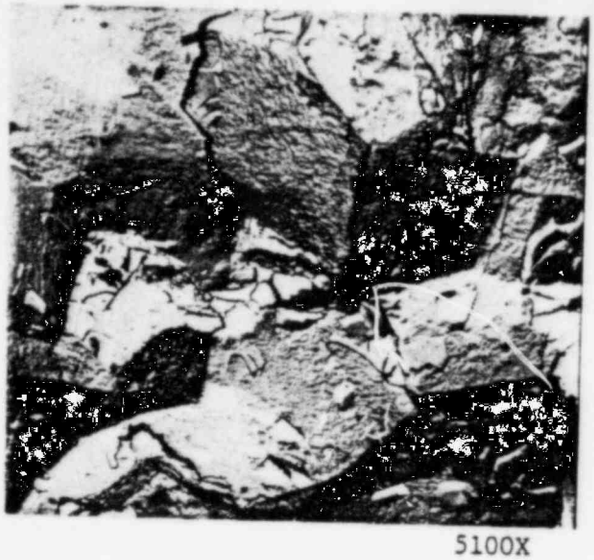

5100X

(a) GENERAL VIEW

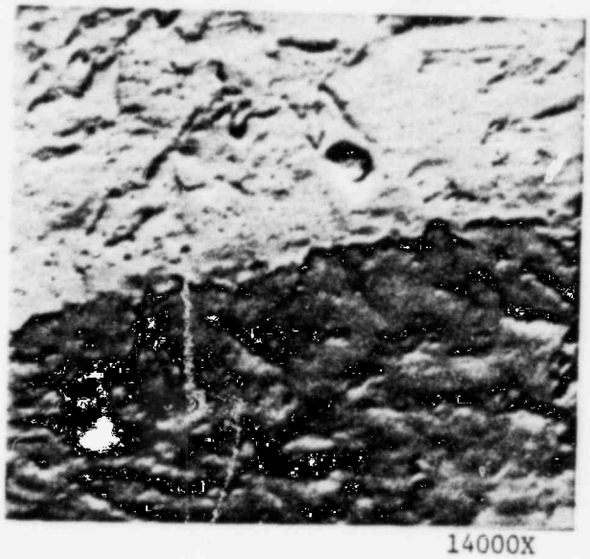

14000X

(b) GRAIN BOUNDARY

12000X

(c) GRAIN BOUNDARY TRIPLE POINT

FIGURE 19. TEM PHOTOMICROGRAPHS OF THE REPLICA OF FRACTURE SURFACE OF SPECIMEN A4 FROM TUBE B-8-25 AFTER DESCALING

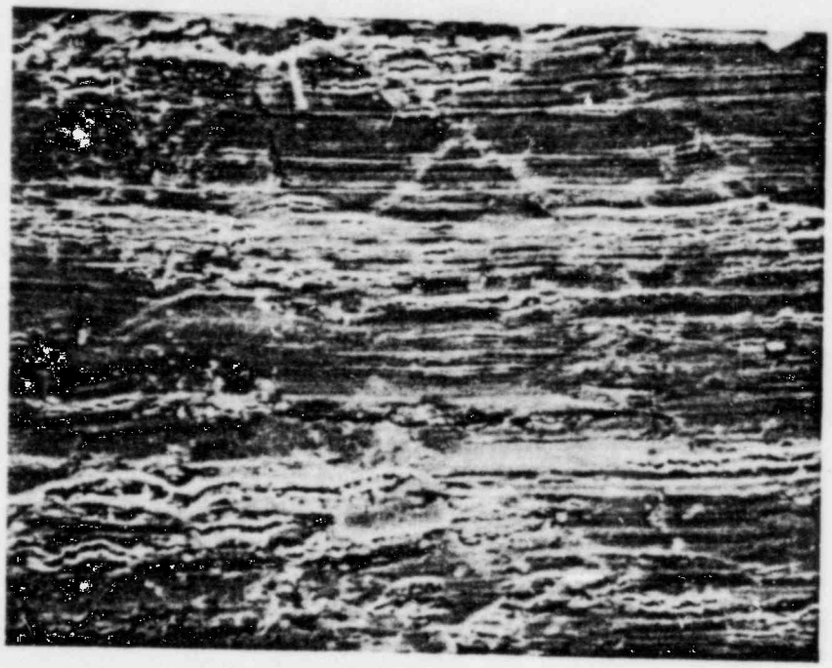

650X

FIGURE 20. SEM PHOTOGRAPH OF THE APEX OF U-BEND OF SPECIMEN A7 FROM TUBE B-8-25

at 5×10^{-10} to 1×10^{-9} torr vacuum. Auger spectra were produced with a scanned electron beam of 5 keV, having a 5 μm spot size. Scanned areas on specimens for auger analysis ranged from 0.5 x 0.5 mm to 1 x 1 mm. Auger electrons emitted from a specimen were analyzed with a hemispherical photomultiplier detector. The Auger spectra of specimens were matched to standards given in "Auger Electron Spectroscopy Reference Manual"* for the identification of elements.

ESCA spectra of specimens were produced with Mg-k_{α} 1254 eV x-rays, from a gun operated at 12 kV and incident at ∿45° onto 1 cm^2 area at sample location. Thus, the area of a specimen analyzed was that exposed to x-rays in the 1 cm^2 region. If the surface area of the exposed specimen was smaller than 1 cm^2, the x-ray photoelectrons for ESCA were produced from the available surface, and the resulting signals were proportionately weaker. The spectra of specimens were interpreted on the bases of standard binding and kinetic energies of electrons given in "Handbook of X-Ray Photoelectron Spectroscopy."**

The A3 surface was analyzed with AES in the as-received condition, and after sputtering away 600, 900, 1200 and 1500Å of the surface film. The AES spectra was taken at several spots on the A3 surface, namely, in the IGC area at tube ID edge, center OD edge and front edge of the specimen. The freshly fractured area of A3 also was analyzed. A quantitative estimation of elemental distribution over the entire A3 fractured surface was determined with ESCA after sputtering 0, 600 and 900Å of the surface film. The results of AES analysis are given in Table 5 and those of the ESCA analysis in Table 6.

The AES detected a host of elements on the fracture surface as shown in Table 5. The elements detected were C, O, Fe, Ni, Cr, S, P, Cl, B, Be, Zr and various fission products of uranium. The most predominant element on the surface was C, its concentration was 90 atom percent in the top layer but decreased to 64.8 percent at 900Å depth.

---

* G. E. McGuire, "Auger Electron Spectroscopy Reference Manual", Plenum Press, NY (1979).

** C. W. Wagner et al, (Eds.), "Handbook of X-Ray Photoelectron Spectroscopy" Perlain Elma Corp., Minn. (1979).

TABLE 5. AES ANALYSIS OF FRACTURE SURFACE OF SPECIMEN A3 FROM TUBE B8-25

Depth Sputtered	Area on Fracture Surface	Elements Detected
None	IGC Center	C, O, Cs, Y, Sn, La
	Fresh Fracture	C
600Å	IGC Center	C, K, B, Sb, P, Be
	IGC Edge	C, K, Be, P, Y, S, B, Ag, Te
	Fresh Fracture	C, Ni
900Å	IGC Edge	C, Ag, Ca, S, P, Be, K, Ca
1200Å	IGC Edge	C, Si, Be, S, Cl, Ar, Rh, Ag, O, Cr
	IGC OD Side	C, Be, Ca, Ag
	IGC ID Side	C, Si, B
	IGC Center	C, Si, B, Ag, O
	Fresh Fracture	C, Ni, Cu, O
1500Å	IGC Center	C, S, Ru, Ag, Cs, O, Be, P
	IGC Edge	C, Si, Be, P, Cl, Ag, Te, O, La

TABLE 6. ESCA ANALYSIS OF FRACTURE SURFACE OF SPECIMEN A3 FROM TUBE B8-25

Depth Sputtered, Å	Surface Composition, atomic percent											
	Ni	Fe	Cr	O	C	S	Ag	Be	Cs	P	Ru	Cu*
None				~10	~90							
600	3.0	1.7	1.1	11.1	75.8							4.6
900	3.4	2.3	1.5	11.8	64.8	0.4	0.3	7.2	0.4	0.5	0.9	6.6

*Cu from copper holder.

The distribution of elements on the fracture surface was extremely nonuniform. Not only the distribution varied with the sputtering depth but also from one spot to the next, which might be only a few micrometers away. Worth pointing out is the heavy concentration, 7.2 atom percent of Be observed at 900 Å depth in ESCA analysis.

The total fracture surface area on A3 specimen was not large enough for very detailed ESCA analysis. Therefore, a second specimen, namely B, was used which consisted of multiple fracture surfaces stacked together, as shown in Figure 21. The results of ESCA analysis are summarized in Tables 7 and 8.

Note that both S and Cl were detected at ∿1 atom percent level up to the 2300 Å depth analyzed. Boron also was detected at this depth in 3.3 atom percent concentration. Carbon as usual was high, 64.2 atom percent at 30 Å, but lower 48.9 atom percent at 2300 Å depth. Note also the very low concentration of oxygen, 20.6 atom percent at 30 Å, which decreased further with depth to 14.9 atom percent at 2300 Å.

The chemical state of the elements, as determined from their respective binding energies in the ESCA spectra, are given in Table 8. Only Cr and Fe are shown to be associated with oxygen. Sulfur was in its reduced state as sulfide, $S^{=}$, (probably as NiS) and C is thought to be in a form similar to graphite.

The ID surfaces of specimens C1 and C2 were only visually examined. The whole surface was covered with dull-color surface film. Along the length of the specimens several brown color decorations also were observed. Each decoration had the appearance of a tree, i.e., it had a main trunk and some spreadout branches, see Figure 22. The brown color decorations gave an appearance of some corrosion attack on the metal surface, underneath the surface film.

Some dark brown circumferential lines (wider than a hair strand) were observed at locations 3.0, 3.5 and 4.0 inch on the C2 specimen. These lines gave an appearance of circumferential cracks, which may have been the cause of EC indications at these locations as reported in Table 2. The specimen was not examined any f ..ier.

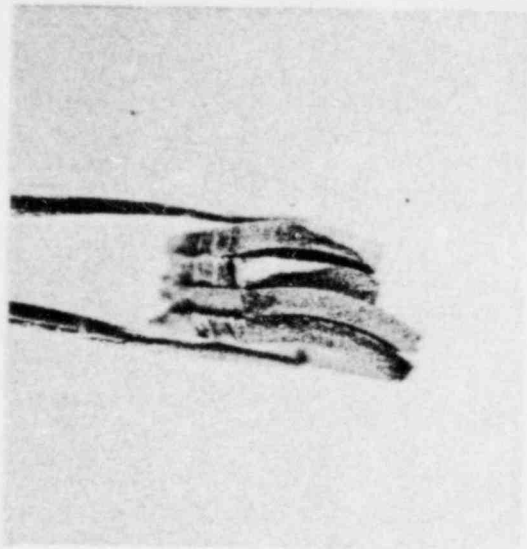

4X

FIGURE 21. PHOTOGRAPH OF SPECIMEN B FROM TUBE B-8-25 SHOWING MULTIPLE FRACTURE SURFACES STACKED TOGETHER FOR ESCA ANALYSIS

TABLE 7. ESCA ANALYSIS OF FRACTURE SURFACE OF SPECIMEN B FROM TUBE B8-25

Depth Sputtered, Å	Surface Composition, atomic percent							
	Ni	Fe	Cr	O	C	Cl	S	B
30	8.9	2.1	2.8	20.6	64.2	0.8	0.6	
150	18.1	3.2	3.6	16.8	58.3	0.6	0.7	
400	15.4	2.8	5.6	18.4	55.6	1.5	0.7	
1100	15.7	3.2	5.1	15.5	59.7	0.7		
2300	21.3	3.8	6.1	14.9	48.9	0.6	1.1	3.3

TABLE 8. ESCA BINDING ENERGIES AND STATES OF ELEMENTS ON SPECIMEN B FROM TUBE B8-25

Depth Sputtered, Å	Ni	Fe	Cr	C	Cl[a]	B[a]	S
30	852.0 Ni	709.0 FeO	576.0 Cr_2O_3	285.0 C			162.0 S^{-2}
150	852.0 Ni	709.0 FeO	576.0 Cr_2O_3				162.0 S^{-2}
400	852.0 Ni	709.0 FeO	576.0 Cr_2O_3		198.0		162.0 S^{-2}
1100						190.0	
2300					198.0	190.0	162.0 S^{-2}

(a) Too low intensity for high resolution.

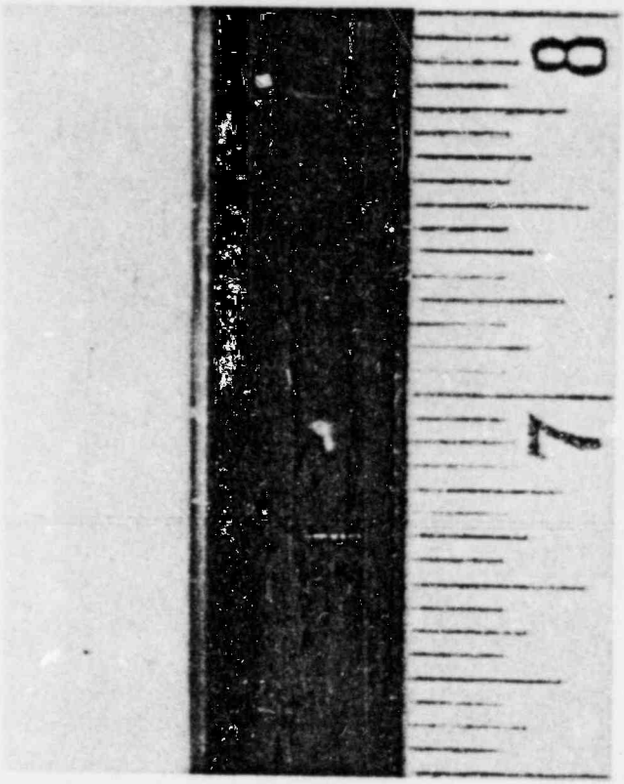

FIGURE 22. A TREE-LIKE BROWN DEPOSIT ON THE ID SURFACE OF TUBE B-8-25

4.2 Tube B-11-23

Short-pull tube B-11-23 was examined using the following techniques:

(1) Visual examination of U-bend slices
(2) Metallographic examination
(3) AES and ESCA examinations of fracture surface film
(4) Wall thickness measurements.

Examination results are summarized in Table 9, using the same format as in Table 3. Details of the results are given below.

Visual examination of U-bend slices from specimen F (i.e., F1 to F4) showed cracks at location 1.25 inch, 180 to 360°. The specimen had an EC indication at 1.0 inch location. The crack penetration was 70 to 100 percent through wall. The matching specimen E (i.e. 0 to 180°) also showed 100 percent through wall crack, see micrograph in Figure 23. An intergranularly attacked area, ~20 percent through wall, was observed on the 0° face of specimen E; the IGA is shown in Figure 24.

A crack in tube B-11-23 at location 2.5 inch, 90 to 270°, was through wall and visible to the unaided eye. A photomicrograph of specimen A containing the above crack is shown in Figure 25. The section of the crack shown is at the 225° circumferatal location on the tube. The crack is clearly intergranular, with IGA spread at least 7 grains deep on either side of the crack. IGA also was observed on the ID surface of the tube, away from the crack, +0.25 to - 0.25 inch, and also on the wall (45° face) opposite to the crack. The IGA in some places was 3 to 4 grains deep as shown in Figure 26. The specimen was examined after an oxalic acid etch, and no IGA was found on the OD surface, either at the 45° location or the 225° crack side location. This clearly indicates that the IGC initiated on the ID side of the tube.

The microstructure of specimen A after a phosphoric acid etch is shown in Figure 27. The grain size ranged between 5 and 50 μm. The average size of grains, when viewed at 100X, corresponded to ASTM No. 7 or 8. Discrete

TABLE 9. EXAMINATION RESULTS OF TUBE B11-23

Specimen Number	Location		Type of Indication	Examination	Result/Comment
	Inches	Degrees			
A	2.0-2.75	45-225	Radiograph, Visual	Metallographic μ Structure	IGC 100% Wall, ID-IGA Discrete Carbide ppt Inter + Intra Granular
B	7.0-7.5	0-360	None	STEM	Sent to MIT
C	2.0-3.0	225-270	Radiograph, Visual	AES/ESCA	Crack Surface High C Some S
D	6.5-7.0	0-360	None	EPR Sensitization	Specimen Mounted But Not Used
E	0-2.0	0-180	EC, Radiograph	Wall Thickness μ Structure	0.0348 min./0.0365 max. IGC 100% Wall 180°, IGA 20% Wall 0°
F (F1-F4)	0-2.0	180-360	EC, Radiograph	Wall Thickness Bend Visual	0.0361 min./0.0377 max.
F1	0-2.0	180-225			1.25, 1.50,~100% Wall
F2	0-2.0	225-270			1.25, 225-250 70% Wall
F3	0-2.0	270-315			1.25, 270-315 70% Wall
F4	0-2.0	315-360			1.25, 315-360 90% Wall
G	7.5-12.0	0-360	EC 10.0	Corrosion Test	Sent to ORNL

100X

FIGURE 23. PHOTOMICROGRAPH OF IGC IN SPECIMEN E FROM TUBE B-11-23

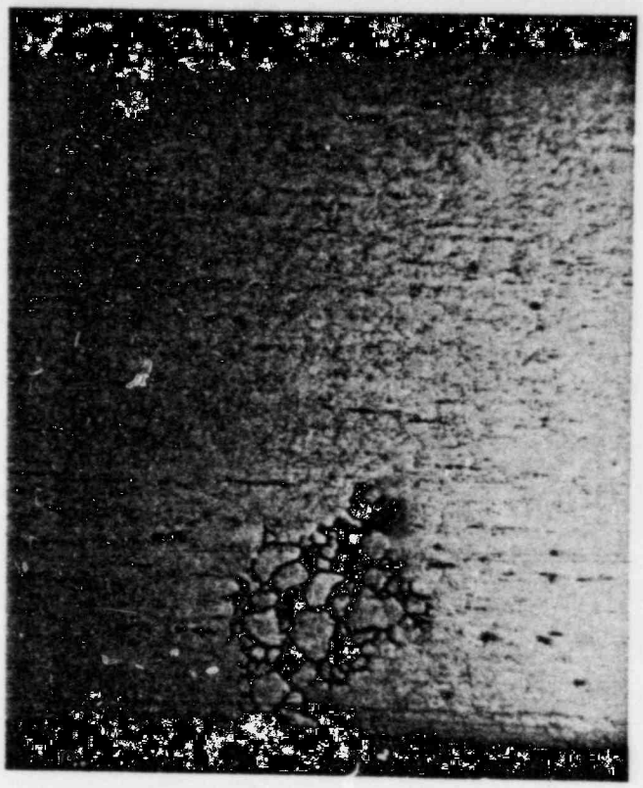

FIGURE 24. PHOTOMICROGRAPH OF IGA IN SPECIMEN E FROM TUBE B-11-23.

FIGURE 25. PHOTOMICROGRAPH OF SPECIMEN A FROM TUBE B-11-23 SHOWING IGC AND SEVERE IGA ON EITHER SIDE OF THE CRACK

60X

FIGURE 26. PHOTOMICROGRAPH OF IGA ON THE ID SURFACE OF SPECIMEN A FROM TUBE B-11-23

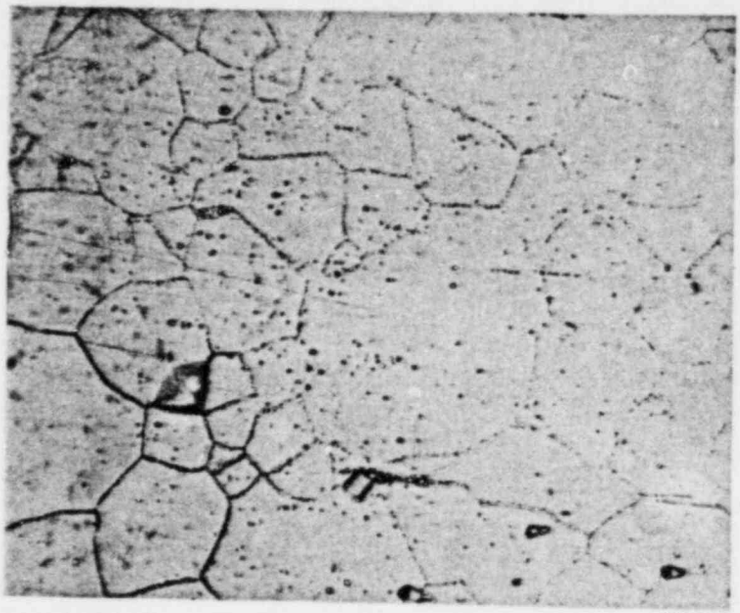

500X

FIGURE 27. PHOTOMICROGRAPH OF THE MICROSTRUCTURE OF SPECIMEN A FROM TUBE B-11-23

chromium carbide precipitates inside the grains and also on the grain boundaries are visible. The grain boundaries already affected by IGA were heavily attacked on etching with phosphoric acid.

The remainder of the above crack contained in specimen C was analyzed by AES and ESCA. Spectra of the as-cut specimen showed C, O and Ni on the fracture surface. The surface was sputtered with 2 KeV argon ion beam, and after removing 20 Å of the surface film, sulfur was detected at one edge of the surface. Carbon on the surface was in very large concentration in comparison to the rest of the elements. Because of the overwhelming concentration of carbon, a quantitative estimation of other elements was not attempted.

The fracture surface was further sputtered and analyzed at 50, 100 and 200 Å depths. With depth, the concentration of C and O decreased but that of Fe, Ni and Cr increased. The concentration of S increased up to 50 Å but decreased thereafter. The analysis was not carried beyond 200 Å depth.

Wall thickness measurement results are given in Table 10 for specimens E and F. The maximum thickness measured was 0.0377 inch and the minimum 0.0348 inch. The thickness was generally 0.001 inch lower in the rolled section than in the unrolled tube.

4.3 Tubes A-23-93, A-88-11 and A-112-5

Short-pull tubes A-23-93, A-88-11 and A-112-5 were examined only visually for defects in the roll transition region, by slitting the upper section (0-2.25 inch) of each tube into eight slices and bending them into a U-shape. Wall thickness measurements, however, were taken of one tube, A-23-93. Tube A-23-93 had an EC indication at location 1.75 inch and tubes A-88-11 and A-112-5 at 1.25 inch.

Results of U-bend examinations of tubes A-23-93, A-88-11 and A-112-5 are summarized, respectively, in Tables 11, 12 and 13. Wall thickness measurements of tube A-23-93 are given in Table 14.

TABLE 10. WALL THICKNESS OF TUBE B11-23

Location, inches	Wall Thickness, inch			
	45° Position	135° Position	225° Position	315° Position
1/8	0.0348	0.0350	0.0368	0.0365
1/4	0.0354	0.0351	0.0361	0.0368
3/8	0.0354	0.0355	0.0364	0.0367
1/2	0.0352	0.0353	0.0362	0.0363
5/8	0.0352	0.0352	0.0364	0.0362
3/4	0.0356	0.0351	0.0364	0.0362
7/8	0.0353	0.0350	0.0368	0.0362
1	0.0355	0.0350	0.0370	0.0365
1-1/8	0.0362	0.0360	0.0372	0.0370
1-1/4	0.0363	0.0359	0.0372	0.0372
1-3/8	0.0364	0.0361	0.0372	0.0371
1-1/2	0.0362	0.0361	0.0373	0.0370
1-5/8	0.0362	0.0361	0.0377	0.0368
1-3/4	0.0365	0.0360	0.0372	0.0370
1-7/8	0.0365	0.0359	0.0372	0.0370

TABLE 11. EXAMINATION RESULTS OF TUBE A23-93

Specimen Number	Location		Type of Indication	Examination	Result/Comment
	Inches	Degrees			
A (A1-A8)	0-2.5		EC 1.75, 20-140 Radiograph Lip Crack	Wall Thickness Slit and Bend Visual	0.0357 min./0.0371 max. 1.5 Pits, No Crack Visible On As Cut Halves
A1	0-2.5	0-45			No Crack
A2	0-2.5	45-90			1.75, 60-90 Crack ~100% Wall
A3	0-2.5	90-135			1.75, 90-135 Crack ~100% Wall, Also Pits
A4	0-2.5	135-180			1.75, 135-140 Crack ~95% Wall
A5	0-2.5	180-225			No Crack
A6	0-2.5	225-270			No Crack, 2.25~270 Pits
A7	0-2.5	270-315			0.25, 270-315 Lip Crack 100% Wall
A8	0-2.5	315-360			No Crack
B	2.5-12	0-360			Reserved for B&W

TABLE 12. EXAMINATION RESULTS OF TUBE A88-11

Specimen Number	Location		Type of Indication	Examination	Result/Comment
	Inches	Degrees			
A (A1-A8)	0-2.5		EC, Radiograph	Slit and Bend Visual	Pits at Several Places
A1	0-2.5	0-45			0.25 Lip Crack
A2	0-2.5	45-90			2.25, 60-90 Crack 90% Wall
A3	0-2.5	90-135			2.25, 90-120 Crack 90% Wall
A4	0-2.5	135-180			1.25, 130-180 Crack ~100% Wall
A5	0-2.5	180-225			1.25, 180-200 Crack ~100% Wall
A6	0-2.5	225-270			0.25 Lip Crack
A7	0-2.5	270-315			No Crack
A8	0-2.5	315-360			0.25 Lip Crack 2.25, 330-360 Crack 80% Wall
B	2.5-12.5				Unused

TABLE 13. EXAMINATION RESULTS OF TUBE A112-5

Specimen Number	Location		Type of Indication	Examination	Result/Comment
	Inches	Degrees			
A (A1-A8)	0-2.5		EC, Radiograph	Slit and Bend Visual	
A1	0-2.5	0-45			1.25, 0-45 Crack ~100% Wall
A2	0-2.5	45-90			1.25, 45-60 Crack 90% Wall, Lip Crack
A3	0-2.5	90-135			No Cracks
A4	0-2.5	135-180			0.25 Lip Crack
A5	0-2.5	180-225			0.25 Lip Crack
A6	0-2.5	225-270			0.25 Lip Crack
A7	0-2.5	270-315			0.25 Lip Crack
A8	0-2.5	315-360			1.0-1.25, 315-360 ~100% Wall
B	2.5-12.5	0-360			Reserved for B&W

TABLE 14. WALL THICKNESS OF TUBE A23-93

Location, inches	Wall Thickness, inch			
	45° Position	135° Position	225° Position	315° Position
1/8	0.0368	0.0361	0.0359	0.0357
1/4	0.0371	0.0360	0.0358	0.0357
3/8	0.0370	0.0359	0.0357	0.0358
1/2	0.0359	0.0360	0.0358	0.0358
5/8	0.0359	0.0358	0.0358	0.0358
3/4	0.0360	0.0360	0.0358	0.0356
7/8	0.0361	0.0363	0.0357	0.0358
1	0.0363	0.0362	0.0358	0.0357
1-1/8	0.0371	0.0365	0.0361	0.0362
1-1/4	0.0369	0.0362	0.0361	0.0365
1-3/8	0.0366	0.0362	0.0362	0.0368
1-1/2	0.0362	0.0362	0.0362	0.0369
1-5/8	0.0368	0.0362	0.0365	0.0368
1-3/4	0.0362	0.0362	0.0370	0.0367
1-7/8	0.0362	0.0361	0.0368	0.0366

Visual examination of tube A-23-93 revealed lip-cracks at location 0.25 inch, 270-315°, and a second crack, nearly through wall, at location 1.75 inch, 60-140°. Some pits, probably due to grain dropping, were also observed at 1.5 inch and 2.25 inch locations. Wall thickness of tube A-23-93 was much more uniform than tube B-11-23. The maximum thickness in tube A-23-93 was 0.0371 inch and the minimum was 0.0357 inch, see Table 14.

Three separate cracks were observed in tube A-88-11. One was a lip-crack at location 0.25 inch, 315-45°, the second crack was at 1.25 inch, 130-200°, and the third crack was at 2.25 inch, probably between 330 and 120°, see Table 12.

Two cracks were observed in tube A-112-5. One was a lip-crack at 0.25 inch, 135-315°. The second crack was nearly through wall at 1.25 inch, 315-60°, see Table 13.

4.4 Tube A-71-126

Long-pull tube A-71-126 was examined with the following techniques:

(1) Visual examination of U-bend slices
(2) Visual examination of ID surface after descaling
(3) Metallographic examination
(4) Tensile test
(5) Alloy composition
(6) EPR sensitization test
(7) AES and ESCA of the ID surface.

Results of these examinations are summarized in Table 15 according to the format of Table 3. Details of the results are given below.

Specimens for visual examination of U-bend slices were taken from three different locations of the tube. The specimen X (X1 to X8) was from location 0-2.0 inch, specimen Y (Y1 to Y4) from 2.0-4.0 inch, and specimen F from 50.5-58.5 inch. Thus, specimen F was from the long-pull section that was well below the tube sheet crevice region.

TABLE 15. EXAMINATION RESULTS OF TUBE A71-126

Specimen Number	Location		Type of Indication	Examination	Result/Comment
	Inches	Degrees			
X (X1-X8)	0-2.0		Radiograph 1.75	Slit and Bend Visual	
X1	0-2.0	0-45			0.25 Lip Crack
X2	0-2.0	45-90			0.25 Lip Crack, 1.0 Pits
X3	0-2.0	90-135			1.0 Pits
X4	0-2.0	135-180			No Cracks
X5	0-2.0	180-225			No Cracks
X6	0-2.0	225-270			Possible IGA
X7	0-2.0	270-315			0.25 Rolled Metal
X8	0-2.0	315-360			0.25 Rolled Metal
Y (Y1-Y4)	2.0-4.0		EC 3.0	Slit and Bend Visual	
Y1	2.0-4.0	0-90			No Cracks
Y2	2.0-4.0	90-180			No Cracks
Y3	2.0-4.0	180-270			No Cracks
Y4	2.0-4.0	270-360			No Cracks
Z	4.0-13.0	0-360			Unused
S	13.0-25.75	0-360			Unused
T	25.75-38.25	0-360			Sent to ORNL
U	38.25-51.0	0-360			Sent to ORNL
A	59.0-60.0	0-180	None	Alloy Composition	0.034% C, 15.3% Cr
B	59.5-60.0	180-360	None	EPR Sensitization	Activation Potential 110 mV (SCE)
C	52.0-52.5	180-360	None	ID AES/ESCA	B (3.5%), Zr (0.3%), S (1.0%), $SO_4^=$ Top/$S^=$ Bottom
D	52.5-59.5	180-360	Radiograph	Visual	Descaled, No Obvious Crack
E	51.0-52.0	180-360	Visual - Gouges	None	Unused
F	50.5-58.5	0-180	Radiograph	ID Bend, Visual	No Cracks (3X Visual)

TABLE 15. (Continued)

Specimen Number	Location		Type of Indication	Examination	Result/Comment
	Inches	Degrees			
G	60.0-68.25	0-360	Radiograph	Tensile Test, Slit Visual	YS 53 KSI, UTS 101 KSI No Other Cracks, Descaled
H	68.25-68.5	0-360	Visual - Gouges	None	Unused
I	53.25-53.75	180-360	Visual - Pits	Transverse Met.	Mechanical Indentations
J	53.75-54.25	180-360	Visual - Pits	Longitudinal Met.	Mechanical Indentations

In specimen X, a lip-crack was observed at 0.25 inch, 0-90°. Some pits were also observed at 1.0 inch, 45-135°. The nature of these pits, i.e., whether they were formed from mechanical damage of the tube or from grain dropping was not obvious. No other crack, beside the lip-crack was found in specimen X. The radiographic indication at 1.75 inch was not confirmed as a crack with visual examination.

No cracks were found in specimen Y, which had an EC indication at 3.0 inch location. Specimen F was a 8.0 inch long slice which was bent into a C-shape over a 4-inch diameter tube and then examined. No crack was found over its entire length.

The ID surface of specimen F, however, before bending was found to be heavily scored practically all over its length. A photograph of the descaled scored surface is shown in Figure 28. The scoring marks were possibly responsible for the defect indications in radiographs, described in Section 3.3.

A general view of the ID surface of the tube section between 51.0 and 60.0 inches, before descaling is shown in Figure 29. Score marks can be seen on all quadrants of the section over its entire length. The mechanical nature of the ID surface defects, as shown in Figures 28 and 29, is fairly obvious from the photomicrographs in Figures 30 and 31. The photomicrograph is Figure 30 is a transverse cross section of specimen J, see Table 15 for their locations. The well defined trapezoidal shape of the indentation in Figure 30, and the crushed grains on the surface at the defect site in Figure 31 are indicative of the mechanical penetration.

Specimen G, location 60.0-68.25 inch, was used for determining the mechanical properties of the tube material. Two bullets (each 3.125 inch long) were inserted in the tube, one at either end, for proper gripping and defining the gage section. Thus the gage section in the specimen between the bullet heads was 2.0 inch. The length of the original 8.25 inch specimen after testing was 9.37 inch, i.e., the total elongation in the specimen was 1.12 inch. Since no reference marks in

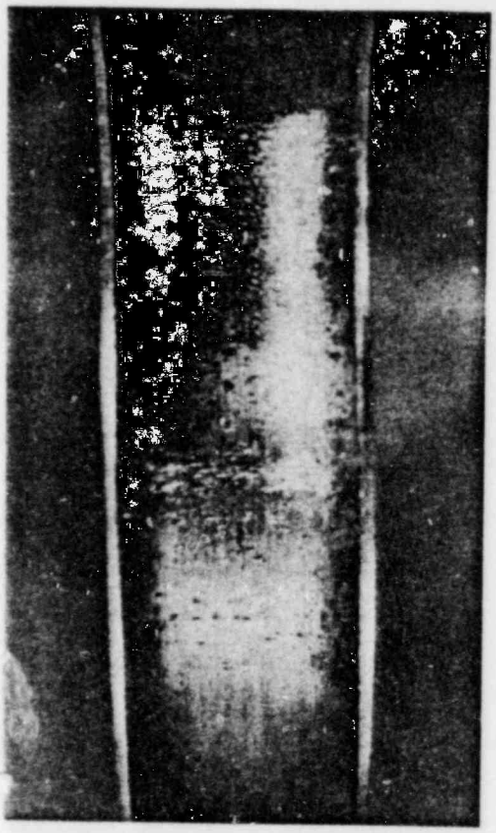

FIGURE 28. PHOTOGRAPH OF THE DESCALED SPECIMEN F FROM TUBE A-71-126 SHOWING HEAVY SCORING

DOCUMENT/ PAGE PULLED

ANO. 8212270056

NO. OF PAGES 1

REASON

☐ PAGE ILLEGIBLE

☐ HARD COPY FILED AT. PDR CF

OTHER _____

☐ BETTER COPY REQUESTED ON ___/___/___

☒ PAGE TOO LARGE TO FILM

☒ HARD COPY FILED AT. PDR (CF)

OTHER _____

☒ FILMED ON APERTURE CARD NO 8212270056-01

FIGURE 29. PHOTOGRAPH OF ID SURFACES OF TWO HALVES OF TUBE A-71-126 BETWEEN 51.0 AND 60.0 INCH BEFORE DESCALING: A) 45° B) 135° C) 225° AND, D) 315° FACE
(SEE NEXT PAGE)

ID 200X

FIGURE 30. PHOTOMICROGRAPH OF THE TRANSVERSE CROSS SECTION OF SPECIMEN I FROM TUBE A-71-126

ID

200X

FIGURE 31. PHOTOMICROGRAPH OF THE LONGITUDINAL CROSS SECTION OF SPECIMEN J FROM TUBE A-71-126

the gage section were made, the true percent elongation in the material could not be calculated. The 0.2 percent offset (a clip gage used) yield strength of the material was determined as 52.8 ksi from 3650 lb. load at yield and the ultimate tensile strength as 101 ksi from the 6990 lb. maximum load attained. The above values are normal for fabricated Inconel 600® tubing.

Specimen A, location 59.0-60.0 inch, was used for determining alloy composition by the X-ray fluoresence technique for all elements except C and N. The C and N were determined with Leco instrument and N by a standard method. The composition of the specimen is given in Table 16. The composition range with 0.034 percent carbon, and less than or equal to 0.01 percent S and P, is normal for an Inconel-600® tubing.

The electrochemical potentiokinetic reactivation (EPR) test was done on specimen B to detect its susceptibility to polythionic acid attack. The EPR technique used was that described by Airey et al of Westinghouse.* The activation peak potential for the alloy was found to be 110 mV (SCE). After the test, the specimen surface was found to be severely attacked in an intergranular mode. The high peak potential of 110 mV suggests, according to the Westinghouse paper, that the tube is in a heat treated condition which makes it extremely susceptible to polythionic acid attack.

The ID surface of specimen C, location 52.0-52.5 inch, was analyzed with ESCA. Results are given in Tables 17 and 18. The prime elements detected on the surface were Ni, Fe, Cr, O, C, B. Zr and S. The concentrations of Fe, Ni and Cr, as might be expected, increased with the sputtering depth, and those of C and O decreased. No definite trend emerged for the minor elements B, Zr and S. It should be noted that the O on ID surface of the present specimens at ∿40 atom percent is about twice as high as that observed on the fractured surface of specimen B from tube B-8-25, and conversely C at ∿20 atom percent is less than half of that on the above fractured surface.

---

* G. P. Airey, et al, Journal of Metals, 33, 28 (1981).

TABLE 16. COMPOSITION OF TUBE A-71-126 ALLOY

Element	Wt. Percent
Ni	balance
Cr	15.3
Fe	9.6
Mn	0.36
Ti	0.21
Co	0.10
Cb	<0.10
Mo	<0.10
Cu	<0.10
Al	<0.10
Si	Not determined properly (~0.2)
P	0.01
S	≤0.01
C	0.034
N	0.013

TABLE 17. ESCA ANALYSIS OF ID SURFACE OF SPECIMEN C FROM TUBE A71-126

Depth Sputtered, Å	Surface Composition, atomic percent							
	Ni	Fe	Cr	O	C	B	Zr	S
None	14.0	2.8	6.9	44.6	28.1	2.3	0.2	1.1
30	18.3	4.1	8.4	43.3	21.4	3.5	0.3	0.6
630	24.1	5.1	10.7	41.1	14.6	3.2	0.3	1.0
1230	25.2	6.8	10.2	39.2	12.9	4.7	0.3	0.8
3630	28.9	8.0	11.7	39.8	10.4	0.0	0.4	0.8

TABLE 18. ESCA BINDING ENERGIES AND STATES OF ELEMENTS ON SPECIMEN C FROM TUBE A71-126

Depth Sputtered, Å	Ni	Fe	Cr	C	S	Ratio $S^{-2}/SO_4^{=}$
None	856.0 $Ni(OH)_2$	711.0 FeOOH	577.0 Cr_2O_3	285.0 C	169.0 SO_4^{-2}	0
30	856.0 $Ni(OH)_2$	711.0 FeOOH	577.0 Cr_2O_3	285.0 C	169.0 SO_4^{-2} 162.0 S^{-2}	1.0
630	852.0 Ni	710.0 FeO	577.0 Cr_2O_3	285.0 C	169.0 SO_4^{-2} 162.0 S^{-2}	2.0
1230	852.0 Ni	710.0 FeO	577.0 Cr_2O_3		169.0 SO_4^{-2} 162.0 S^{-2}	2.0
2430	852.0 Ni 855.0 NiO	710.0 FeO	577.0 Cr_2O_3		162.0 S^{-2}	> 10
3630	852.0 Ni 855.0 NiO	710.0 FeO	577.0 Cr_2O_3			> 10

4.5 Tube A-146-6

Short-pull tube A-146-6 was examined using the following techniques:

(1) Visual and photographic examinations of the ID surface
(2) Microstructure and microhardness measurements
(3) EPR sensitization test
(4) Metallographic and SEM examinations
(5) Electron microprobe analysis of a pit
(6) XRD analysis of ID surface scrapings
(7) AES, ESCA and SIMS analysis of ID surface.

Results of various examinations are summarized in Table 19 using the same format as in Table 3. Details of various results are presented below.

The whole segment of tube A-146-6 was slit into two halves, and their ID surfaces were examined visually and were photographed. The photographs are shown in Figure 32. The ID surface was dull in appearance and it was covered with thin deposits. Several spots were decorated with brown color irregular patterns; these appear as dark patterns in Figure 32. These decorations gave the impression that corrosion (or IGA) had occurred at several points on the tube surface, and the corrosion product had seeped around them and produced these patterns.

The patterns described here are similar to those shown in Figure 22 from tube B-8-25, and described previously as tree decoration. A minor difference between the two is that the lines forming the pattern in Figure 22 are narrower than the corresponding lines in Figure 32. The reason for their appearance on the tube surface, however, is probably the same.

The microstructure examination and microhardness measurements were done on specimen B, location 0.5-1.5 inch. The microstructure of

TABLE 19. EXAMINATION RESULTS OF TUBE A146-6

Specimen Number	Location		Type of Indication	Examination	Result/Comment
	Inches	Degrees			
A	1.0-1.5	0-135	EC 1.25, Visual	TEM	A not Used, Substituted by B8-25 (A4)
B	0.5-1.5	0-180	None	μ Structure μ Hardness	Discrete Carbide ppt. No Continuous Network DPH Max. 270/Min. 170
C	8.0-9.0	180-360	EC 8.25, Visual 360	Longitudinal Met.	IGC 8.25, 100% Wall Both Edges
D	10.0-10.75	180-360	EC 10.5, Visual	ID SEM, Met.	10.5 Pit + IGC, 100% Wall
E	8.25-8.75	0-135	EC 8.5, Visual	ID AES/ESCA	3100 Å S (low) O (46%) C (8%) B (3%) Zr (0.2%)
F (F1-F11)	0-5.5 (0.5 x 11 = 5.5)	225-360	Pits, Visual	ID SIMS/ESCA	F2, 3400 Å S (0.7%) O (33%) C (19%) B (4%) Zr (0.3%) F11, 3500 Å S (1.2%) O (41%) C (6%) B (8%) Zr (0.3%) Ni, NiO, FeO, Cr_2O_3, $S^=$
G	5.5-6.5	180-360	Pits, Visual	Microprobe ID	S and Ti in Pit
H	10.75-11.25	180-360	None	EPR Sensitization	Activation Potential 110 mV (SCE)
I	5.25-5.5 (Part of F11)	300-360	Pits, Visual	XRD	Unknown Spinels, Ni_3TiO_5
J	1.0-1.5 (F3 Specimen)	180-360	CD Deposit, Visual	Transverse Met.	No Defect Under Deposit, No IGA ID or OD
K	2.0-2.5 (F5 Specimen)	300-360	OD Deposit, Visual	Longitudinal Met.	No Defect Under Deposit, No IGA ID or OD
L	1.5-8.25	0-180	Tree Decoration, Visual	None	Specimen Descaled
M	8.75-12.25	0-180	Tree Decoration, Visual	None	Specimen Descaled

FIGURE 32. PHOTOGRAPHS OF ID SURFACES OF TWO HALVES OF TUBE A-146-6; A) 315° B) 225° C) 135° AND, D) 45° FACE (SEE NEXT PAGE)

DOCUMENT/ PAGE PULLED

ANO. 8212270056

NO. OF PAGES 1

REASON

☐ PAGE ILLEGIBLE

☐ HARD COPY FILED AT: PDR CF

OTHER _____

☐ BETTER COPY REQUESTED ON ___/___/___

☒ PAGE TOO LARGE TO FILM

☒ HARD COPY FILED AT: PDR CF

OTHER _____

☒ FILMED ON APERTURE CARD NO 8212270056-02

the alloy is shown in Figure 33 from three different sub-locations, i.e., rolled region, roll transition region, and the unrolled region. There is no noticeable difference between the three microstructures. In all three, the grain size is the same, and the carbide precipitates are discrete over grain boundaries and inside grains. No continuous network of carbide is visible in Figure 33.

Microhardness values at 180° face of specimen B, taken at approximately 1/8 inch intervals are shown in Figure 34. Knoop diamond pyramid hardness readings at any sublocation was taken every 4 mils starting at ∿2 mils from the ID edge of the tube. The highest values were in the rolled section of the tube (location numbers 1, 0.5 inch, to 5, 1.0 inch, in Figure 34) near the ID, the maximum was 270. In the roll transition region (location number 6, 1.1 inch) the maximum value at ID was only 210. The maximum value below the roll transition region was <200. These values are considered normal for fabricated Inconel-600® tubes, and the rolled region of the tube is not excessively cold worked.

An EPR test was done on specimen H from location 10.75-11.25 inch. The activation peak potential was obtained at 110 mV (SCE), This value is the same as that obtained for specimen B of tube A-71-126. According to the criterion used before, tube A-146-6 is extremely susceptible to IGA by polythionic acid.

Specimen C, location 8.0-9.0 inch, had a visible crack and also an EC indication at 8.25 inch. Brown color patterns were present on either side of the crack. Figure 35 is a photomicrograph of the crack, which is intergranular and 100 percent through wall.

A defect associated with another brown color decoration was selected for SEM and metallographic examinations. Some white color deposits also were present at a few places over the decoration. The area selected was specimen D from location 10.0-10.75 inch, which had an EC indication at 10.5 inch.

A SEM photograph of an area including the white deposit is shown in Figure 36. The surface appears crusty around the white deposit. The specimen was then descaled and re-examined. Several areas on the surface were found to have pits and severe IGA. Pits appear to be in places where white deposits were present on the surface before descaling of the specimen. One such pit is shown in Figure 37.

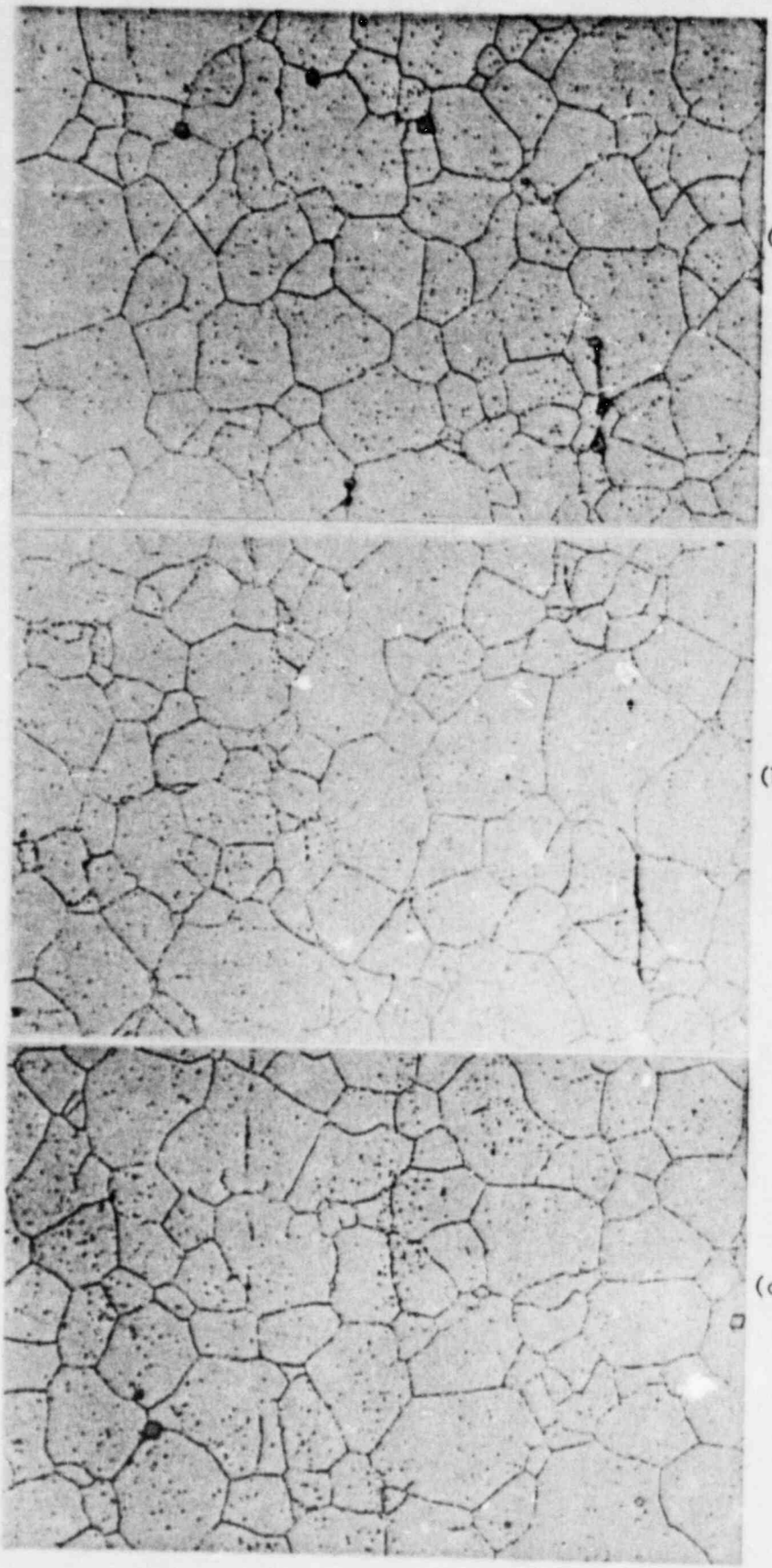

(a) ROLLED REGION

(b) ROLL TRANSITION REGION

(c) UNROLLED REGION

500X H_3PO_4 Etch

FIGURE 33. PHOTOMICROGRAPHS OF THE MICROSTRUCTURE OF THREE DIFFERENT REGIONS OF SPECIMEN B FROM TUBE A-146-6

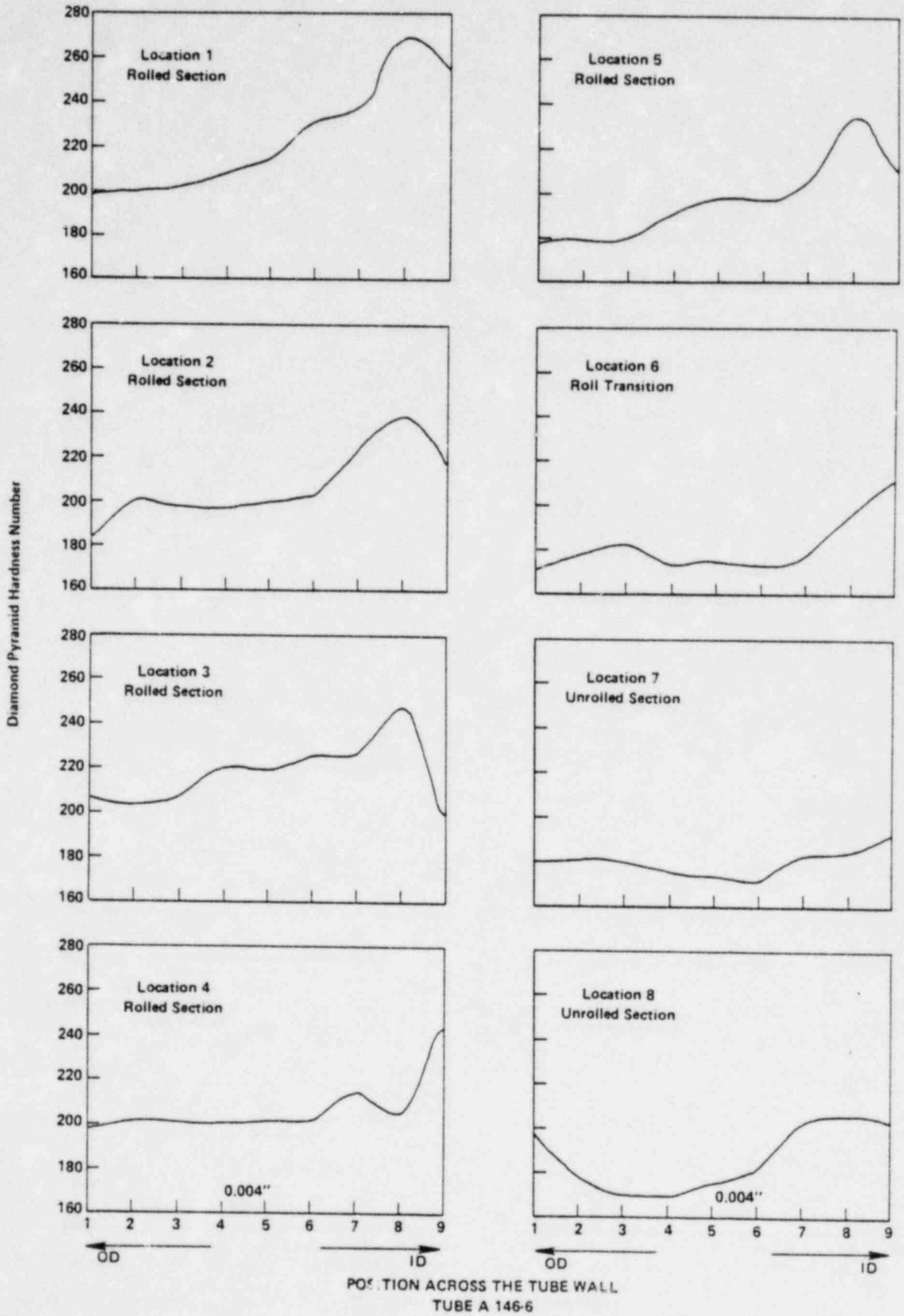

FIGURE 34. MICROHARDNESS VALUES AT 8 DIFFERENT SUB-LOCATIONS ON SPECIMEN B FROM TUBE A-146-6

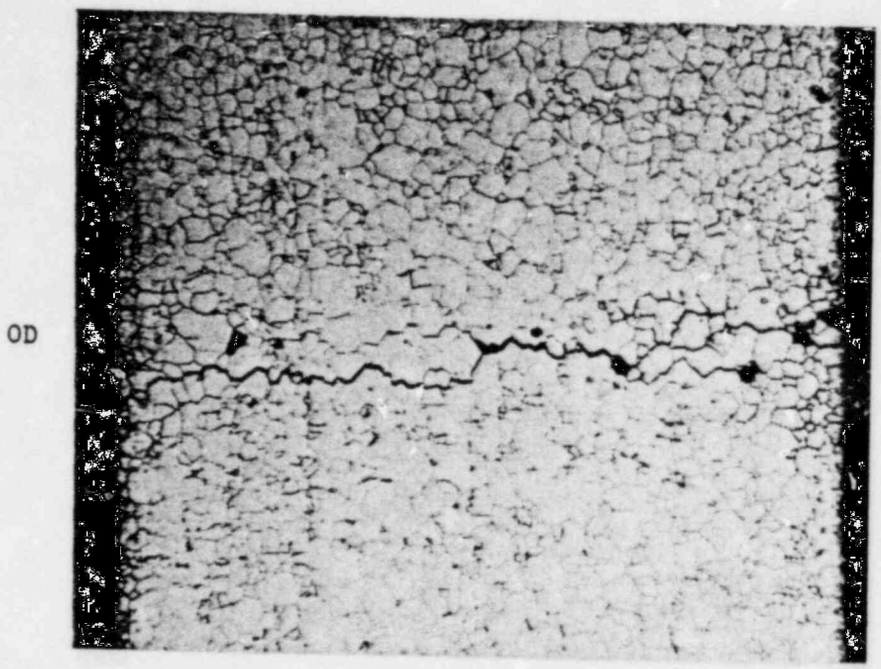

FIGURE 35. PHOTOMICROGRAPH OF THROUGH WALL IGC IN SPECIMEN C FROM TUBE A-146-6

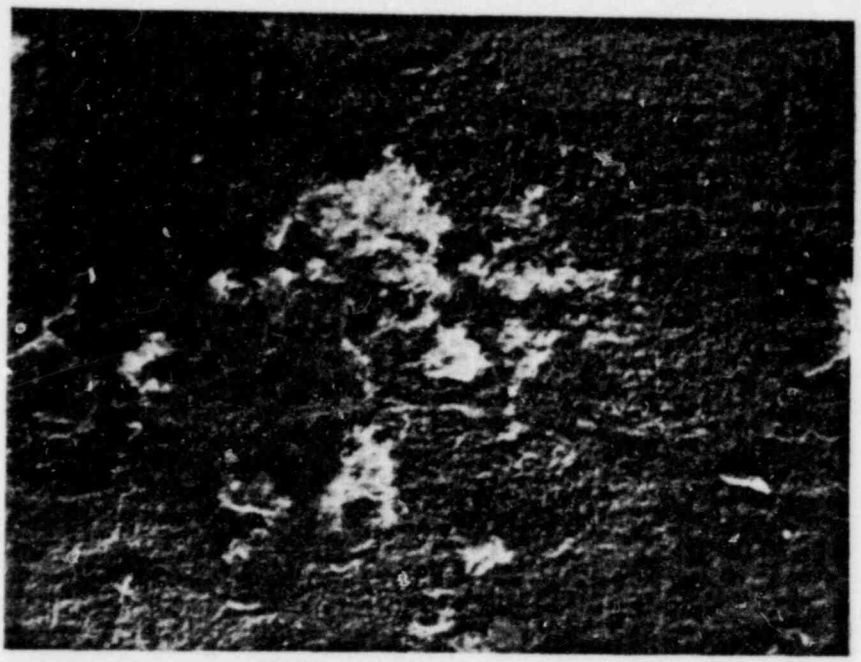

135X

FIGURE 36. SEM PHOTOMICROGRAPH OF A BROWN SPOT AND WHITE DEPOSIT ON THE ID SURFACE OF SPECIMEN D FROM TUBE A-146-6

140X

FIGURE 37. SEM PHOTOGRAPH OF AN IGA PIT ON DESCALED SPECIMEN D FROM TUBE A-146-6

The specimen was further cross sectioned very carefully (in the transverse direction with respect to the tube axis) through one of the large pits for metallographic examination. A photomicrograph of the cross sectioned pit is shown in Figure 38. A through-wall IGC running from the bottom of the IGA pit is clearly visible in Figure 38.

From the examination of specimen C and specimen D, it is fairly certain that the crusty brown deposits and the white deposits on the ID surface are corrosion products. These were either released from the IGA areas and solidified on the surface, or they were formed after the released corrosion product reacted with the tube surface.

A deposit similar to that shown in Figure 36 was cross sectioned and metallographically prepared for electron microprobe analysis. This was specimen G from location 5.5-6.5 inch, which had no EC defect indication. A back-scattered electron image of the ID surface of the specimen is shown in Figure 39. A pit under the deposit is clearly visible.

X-ray images of the specimen for elements Ti, S, Cr, Ni and Fe also are shown in Figure 38. The deposit inside the pit appears to be rich in Cr and Ti, but depleted in Ni and Fe with respect to the base metal. Sulfur is clearly present in all of the deposit. X-ray image of Cl was attempted, but no Cl was detected on the specimen.

These results again indicate that some corrosion product(s), e.g., Fe^{++} released from the pit may have precipitated in the form of oxide (or hydrated oxide) giving rise to the brown color patterns seen on the ID surface.

Some surface deposits, similar to that shown in Figure 36, were scraped from specimen I, location 5.25-5.5 inch, for XRD analysis. XRD patterns obtained indicated Fe, Ni, Cr, some unknown spinels and Ni_3TiO_5 (pattern no. 30-865). No sulfur compound matched any of the XRD patterns.

ESCA results for quantitative analysis of the surface deposits of specimens F2, F11 and E are given, respectively, in Tables 20, 21 and 22. The distribution of Fe, Ni and Cr on the three specimens at nearly the same sputtering depth were not significantly different. In all three cases, Fe, Ni and Cr increased with the sputtering depth, as might be expected.

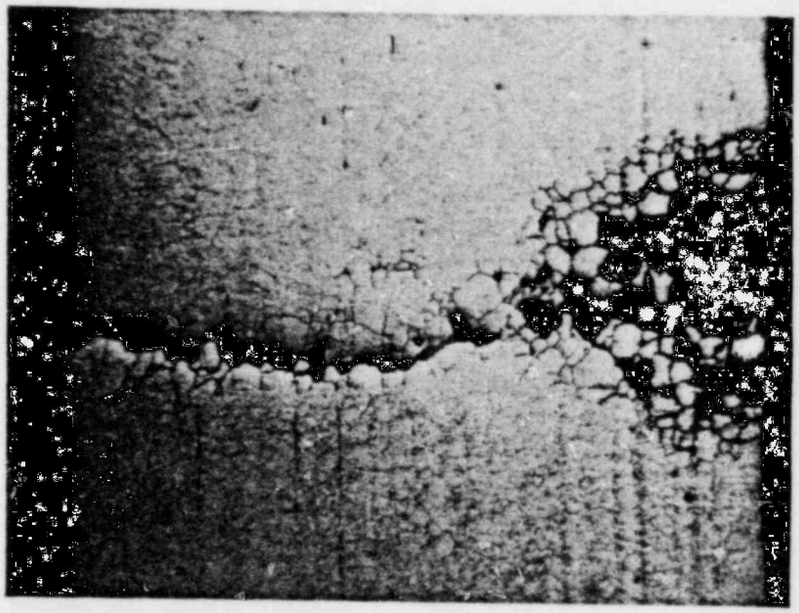

FIGURE 38. PHOTOMICROGRAPH OF THE CROSS SECTION OF A PIT IN SPECIMEN D FROM TUBE A-146-6

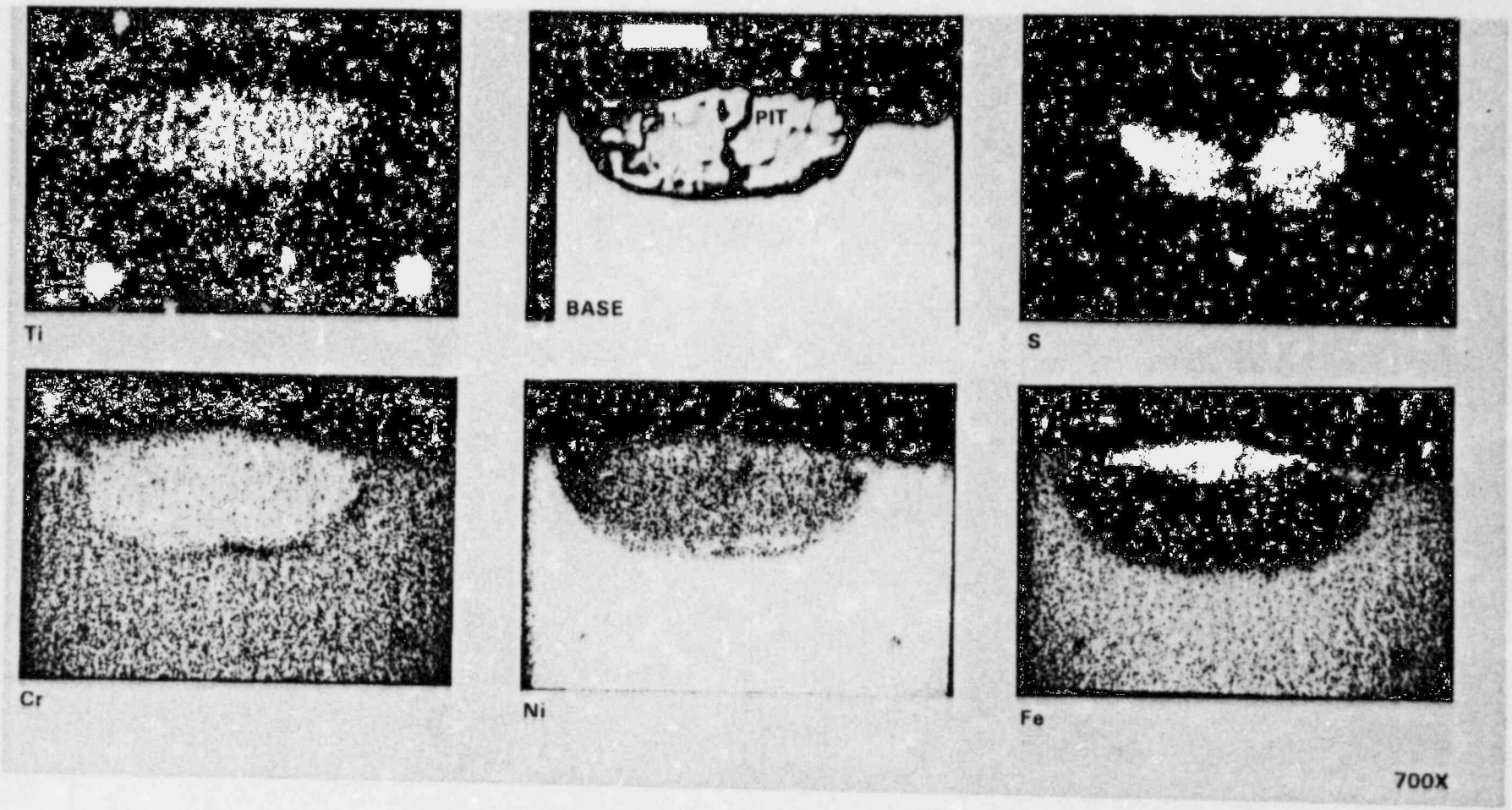

FIGURE 39. BACK SCATTER ELECTRON IMAGE AND X-RAY IMAGES OF ELEMENTS Ti, S, Cr, Ni AND Fe OF A PIT IN SPECIMEN G FROM TUBE A-146-6

TABLE 20. ESCA ANALYSIS OF ID SURFACE OF SPECIMEN F2 FROM TUBE A146-6

Depth Sputtered, Å	Surface Composition, atomic percent							
	Ni	Fe	Cr	O	C	B	Zr	S
None	5.5	3.7	4.1	43.3	39.5	3.8	0.2	
30	7.6	6.6	5.1	39.7	36.5	4.2	0.2	
530	10.9	7.6	6.3	35.3	33.9	4.9	0.2	0.9
1200	15.0	7.4	4.6	33.6	34.3	4.3	0.2	0.6
2400	24.9	8.8	7.6	32.7	22.3	3.2	0.2	0.3
3400	24.3	8.1	8.4	33.4	19.9	4.9	0.3	0.7

TABLE 21. ESCA ANALYSIS OF ID SURFACE OF SPECIMEN F11 FROM TUBE A146-6

Depth Sputtered, Å	Surface Composition, atomic percent							
	Ni	Fe	Cr	O	C	B	Zr	S
None	17.1	4.1	3.7	47.9	21.9	4.2	0.1	0.9
30	18.6	7.2	5.1	45.1	15.4	7.2	0.2	1.2
530	22.0	6.7	6.0	45.2	12.4	6.4	0.2	1.0
1130	25.2	8.5	6.7	39.8	11.5	6.6	0.2	1.5
2330	24.8	9.5	7.5	41.6	8.1	7.4	0.2	0.9
3530	25.6	9.7	7.6	40.9	6.5	8.3	0.3	1.2

TABLE 22. ESCA ANALYSIS OF ID SURFACE OF SPECIMEN E FROM TUBE A146-6

Depth Sputtered, Å	Surface Composition, atomic percent							
	Ni	Fe	Cr	O	C	B	Zr	S
None	8.9	3.9	5.6	68.3	13.4			
350	12.5	6.5	6.0	57.8	17.3			
600	13.9	4.0	6.9	58.9	16.3			
1100	27.7	8.2	6.4	44.6	9.9	3.9		
1600	28.3	8.7	7.3	43.5	7.7	4.3		
2100	26.1	8.2	7.0	44.2	8.4	6.2		
3100	22.0	8.6	12.1	46.3	7.7	3.2	0.2	

AES/ESCA analyses were performed on the ID surface of three different specimens, namely, F2, F11 and E. Locations of these in the above order were 0.5-1.0 inch, 5.0-5.5 inch and 8.25-8.75 inch. AES was used in conjunction with ESCA only to spot check the presence of various elements on the surface. Therefore no separate results were obtained with AES and none are reported here.

Oxygen on specimen F2 at 30 Å depth was 39.7 atom persent and marginally decreased with sputtering to 33.4 atom percent at 3400 Å depth. Similarly, oxygen or specimen F11 at 30 Å was 45.1 atom percent and 40.9 atom percent at 3530 Å. On specimen E, oxygen was 57.8 atom percent at 35 Å and 46.3 atom percent at 3100 Å. The order of oxygen concentration on the three specimens was the same, i.e., 30 to 60 atom percent. With sputtering, the total drop was minimal.

The C concentration on three specimens decreased noticeably with sputtering, see Tables 20 to 22. The concentration dropped from 36.5 to 19.9 for F2, 15.4 to 6.5 for F11 and 17.3 to 7.7 atom percent for E. Specimen F2 had nearly twice as much C on the surface as on F11 or E.

Boron concentration on all three specimens ranged between 3.2 and 8.3 atom percent. Similarly Zr was about 0.2 atom percent on the specimens.

Sulfur on specimen F2 fluctuated between 0.9 and 0.7 atom percent, and on specimen F11 between 1.5 and 0.9 atom percent. Sulfur on specimen E was detected by AES at the depths investigated but the concentration was not high enough ($<$0.1 atom percent) for detection by ESCA.

Binding energies of elements and their chemical states as determined by ESCA analysis are given in Tables 23 to 25 for specimens F2, F11 and E, respectively. The top layer, 0 to $\sim$30 Å, of the surface in each case contained hydrated forms of oxides of Fe and Ni, i.e., FeOOH and $Ni(OH)_2$. The most probable form of Cr on the surface was Cr_2O_3; however, the possibility of CrOOH cannot be ruled out.

With some sputtering, the prominent forms of Fe, Ni and Cr oxides on the surface were determined to be FeO, NiO and Cr_2O_3. Nickel also was present in its elemental form.

TABLE 23. ESCA BINDING ENERGIES AND STATES OF ELEMENTS ON SPECIMEN F2 FROM TUBE A146-6

Depth Sputtered, Å	Ni	Fe	Cr
None	855.4 $Ni(OH)_2$	710.8 FeOOH	576.4 Cr_2O_3 or CrOOH
30	855.4 $Ni(OH)_2$	710.8 FeOOH	576.4 Cr_2O_3
530	852.2 Ni 854.8 NiO	709.9 FeO	576.6 Cr_2O_3
1200	852.2 Ni 854.8 NiO	709.9 FeO	576.6 Cr_2O_3
2400	852.2 Ni 854.8 NiO	709.9 FeO	576.6 Cr_2O_3
3400	852.2 Ni 854.8 NiO	709.9 FeO	576.6 Cr_2O_3

TABLE 24. ESCA BINDING ENERGIES AND STATES OF ELEMENTS ON SPECIMEN F11 FROM TUBE A146-6

Depth Sputtered, Å	Ni	Fe	Cr	C	S	Ratio S^{-2}/SO_4
None	856 $Ni(OH)_2$	714	517 Cr_2O_3	285 C 287 CH_3CH_2O	168 SO_4^{-2}	0
30	856 $Ni(OH)_2$	711 FeOOH	577 Cr_2O_3	285 C	162 S^{-2} 169 SO_4^{-2}	1.4
520	852.2 Ni 855.6 NiO	710 FeO	577 Cr_2O_3	285 C	162 S^{-2} 169 SO_4^{-2}	3
1130	852.3 Ni 855.0 NiO	710 FeO	577 Cr_2O_3	285 C	162 S^{-2} 169 SO_4^{-2}	4
2330	852.3 Ni 855.0 Ni	710 FeO	577 Cr_2O_3	285 C	162 S^{-2}	> 10
3530	852.3 Ni 859.0 NiO	710 FeO	577 Cr_2O_3		162 S^{-2}	> 10

TABLE 25. ESCA BINDING ENERGIES AND STATES OF ELEMENTS ON SPECIMEN E FROM TUBE A146-6

Depth Sputtered, Å	Ni	Fe	Cr
None	855.6 $Ni(OH)_2$	711 FeOOH	576.6 Cr_2O_3
35	852.1 $Ni(OH)_2$	711 FeOOH	576.6 Cr_2O_3
600	852.1 Ni 854.6 NiO	710 FeO	576.7 Cr_2O_3
1100	852.1 Ni 854.6 NiO	710 FeO	576.3 Cr_2O_3
1600	852.1 Ni 854.6 NiO	710 FeO	576.1 Cr_2O_3
2100	852.1 Ni 854.6 NiO	710 FeO	576.1 Cr_2O_3
3100	852.1 Ni 854.6 NiO	710 FeO	576.1 Cr_2O_3

The binding energy of C suggests that it is present as either graphitic carbon or bonded in long chain hydrocarbons.

The S form on the top layer of specimen F11 was $SO_4^=$, but immediately after some (30 Å) sputtering sulfide, $S^=$, was also revealed. With further sputtering, the ratio of $S^=$ to $SO_4^=$ progressively increased, see Table 24. The S forms on specimens F2 and E are thought to be the same as on F11.

Specimen F2 was examined by SIMS after the ESCA studies, i.e., after ion sputtering to 3600 Å depth. The SIMS data were taken while sputtering with 1μ ampere argon ion beam. The ion mass spectra were investigated from two areas on the surface. The areas used were (1) an apparent shallow pit and (2) a bright metallic spot. The principal ions detected were Cr, Fe, Ni, Cr^O, Al, masses 69 and 70, with intermittent detection of B and S_2.

Plots of ion intensity on a relative log scale versus approximate sputtering depth are shown in Figure 40 for the two areas investigated. In the pitter area, there was little change in the intensities of mass 69, Fe, Ni, mass 70, CrO and Al up to the sputtered depth of ∿2μm. Sulfur, however, did go through a maximum at ∿1.5 μm and then decreased.

In the metallic area, practically all ions showed a decreasing trend with sputtering up to ∿1μm. Mass 70, however, went through a minimum at ∿0.5μm depth but then returned to the original value.

The masses 69 and 70 are ascribed to hydrocarbons with possible species of cyclopentane $C_5H_{10}^+$ and its radical $C_5H_9^+$. Such hydrocarbon could be the source of carbon found in the ESCA spectra.

All the examinations and their results described heretofore pertained to the investigation of the ID surface of tube A-146-6. However, two specimens, I and J, were metallographically examined with special attention to the OD surface. Specimen I was from location 5.25-5.5 inch and J from location 1.0-1.5 inch. These two were selected for examination because they had deposits on the OD surface.

Metallographic examinations of the above two specimens showed no defects or IGA under the deposits or at any other locations in the cross sections examined.

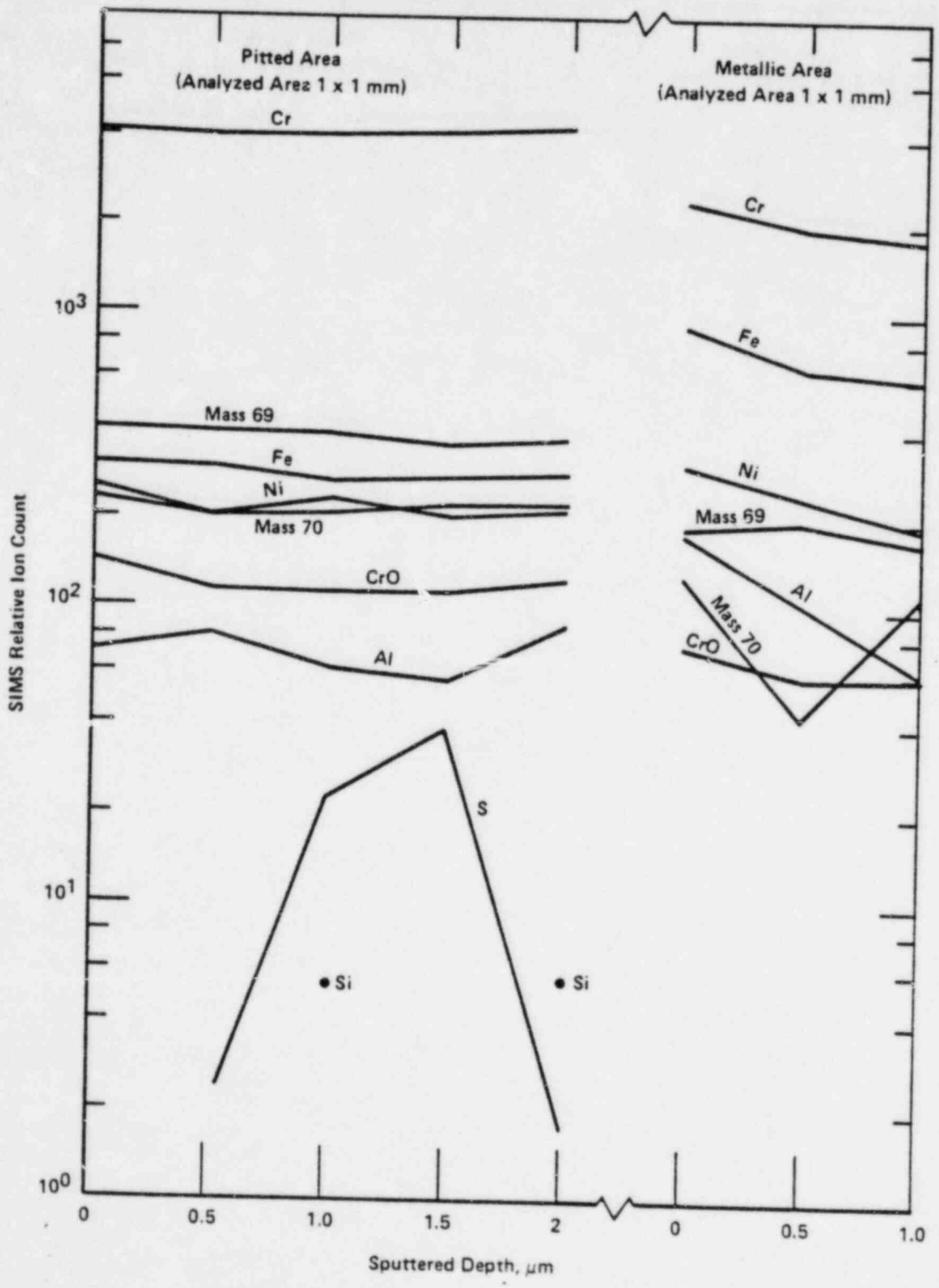

FIGURE 40. RELATIVE ION COUNT IN SIMS VERSUS APPROXIMATE SPUTTERED DEPTH ON THE ID SURFACE OF SPECIMEN F2 FROM TUBE A-146-6

4.6 Tube A-146-8

Short-pull tube A-146-8 was examined using the following techniques:

(1) Visual and photographic examinations
(2) Microstructure and microhardness measurements
(3) EPR sensitization test
(4) SEM and EDAX examinations of ID surface and a fracture fact
(5) Metallographic examinations.

Results of all examinations are summarized in Table 26 using the same format as in Table 3. Details of these results are presented below.

The whole segment of tube A-146-8 was slit into two halves. Their ID surfaces were examined visually and were photographed. The photographs are shown in Figure 41. The features described for tube A-146-6 also were observed on tube A-146-8, namely, dull color surface, deposits on surface, and brown decorations. Some scored areas also are visible in the photograph.

Specimen B from location 0.5-1.5 inch was used for examination of the microstructure and making microhardness measurements.

Photomicrographs of the etched specimen from three different regions of the tube, namely, rolled region, roll transition region, and the unrolled region are shown in Figure 42. The grain size in all three regions is the same; similarly, the carbide decoration of grains and grain boundaries. No continuous networks of carbides were observed. The microstructure of this tube is identical to that of tubes A-71-126 (Figure 31) and A-146-6 (Figure 33).

The microhardness measurements on specimen B were done in the same way as on tube A-146-6. Results for tube A-146-8 are shown in Figure 43. The maximum value, DPH 241, was obtained on the ID surface in the rolled region, and the minimum value, DPH 170, in the mid wall section of the roll transition region. These values again suggest that the tube was not excessively cold worked in any region.

TABLE 26. EXAMINATION RESULTS OF TUBE A146-8

Specimen Number	Location		Type of Indication	Examination	Result/Comment
	Inches	Degrees			
A	0-0.5	0-180	Radiograph, Visual	Longitudinal Met.	U Shape IGC
B	0.5-1.5	0-180	Radiograph, 1.0	μ Structure μ Hardness	Discrete Inter- + Intragranular Carbide ppt No IGA on ID or OD, DPH 241 Max./183 Min.
C	0-0.25	180-360	Visual U Shape	Transverse Met.	3 IGC, ~ 100% Wall
D	0.75-1.25	180-360	None	EPR Sensitization	Not Used, Substituted by L
E1	3.5-4.5	90-180	EC 3.75, Tree Decoration	Longitudinal Met.	IGC, 70% Wall, Microstructure As B No ID or OD IGA
E2	3.5-4.5	0-90	EC 3.75, Tree Decoration	SEM/EDAX	IGC, Fluffy Deposit on Fracture Face S and Ti
F	3.5-4.25	180-360	EC 3.75, Tree Decoration	Transverse Met.	No Defect Detected; No IGA ID or OD
G	8.5-9.0	0-180	None	Longitudinal Met.	IGA 0.004 in. Deep/0.015 in. Wide at ID
H	8.5-9.0	180-360	None	Transverse Met.	No Defect
I	6.75-7.25	0-180	Visual Pits	SEM/EDAX	Pits-IGA, ID Crust, S (7.8%), Ti (2.7%), Ca (0.1%)
J	10.5-11.(	180-360	Visual Scratch!	Longitudinal Met.	No Defect
K	5.75-6.25	0-180	Visual Tree Decoration	SIMS	Not Used
L	0.25-0.75	180-360	None	EPR Sensitization	Activation Potential, 125 mV (SCE)
M	1.5-2.25	0-180	OD Deposit	Longitudinal Met.	No Defect Under Deposit, No IGA ID or OD
N	3.0-3.5	0-180	OD Deposit	Transverse Met.	No Defect Under Deposit, No IGA ID or OD

FIGURE 41. PHOTOGRAPHS OF ID SURFACES OF TWO HALVES OF TUBE A-146-8; A) 45° B) 135° C) 225° AND, D) 315° (SEE NEXT PAGE)

DOCUMENT/ PAGE PULLED

ANO. 8212270056

NO. OF PAGES 1

REASON

☐ PAGE ILLEGIBLE

☐ HARD COPY FILED AT. PDR CF

OTHER _____

☐ BETTER COPY REQUESTED ON __/__/__

☒ PAGE TOO LARGE TO FILM

☒ HARD COPY FILED AT. PDR (CF)

OTHER _____

☒ FILMED ON APERTURE CARD NO 8212270056-03

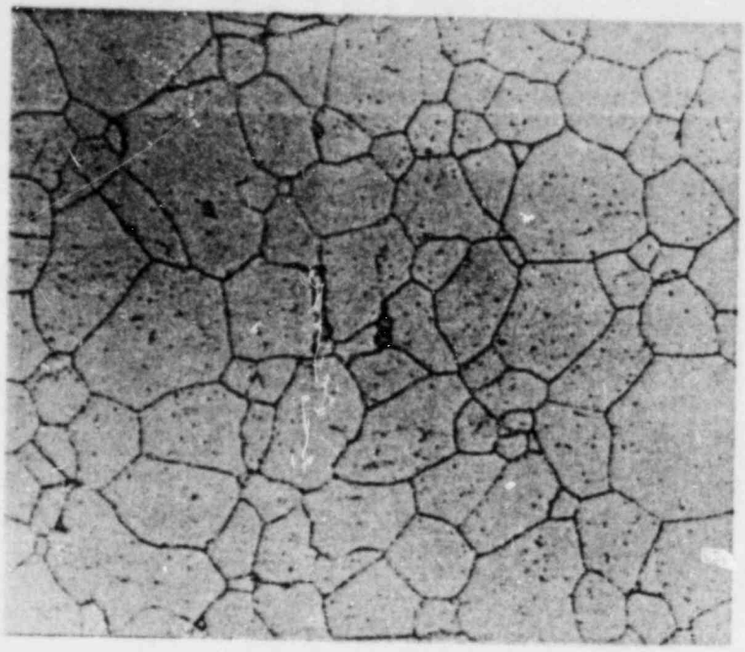

(a) ROLL TRANSITION REGION

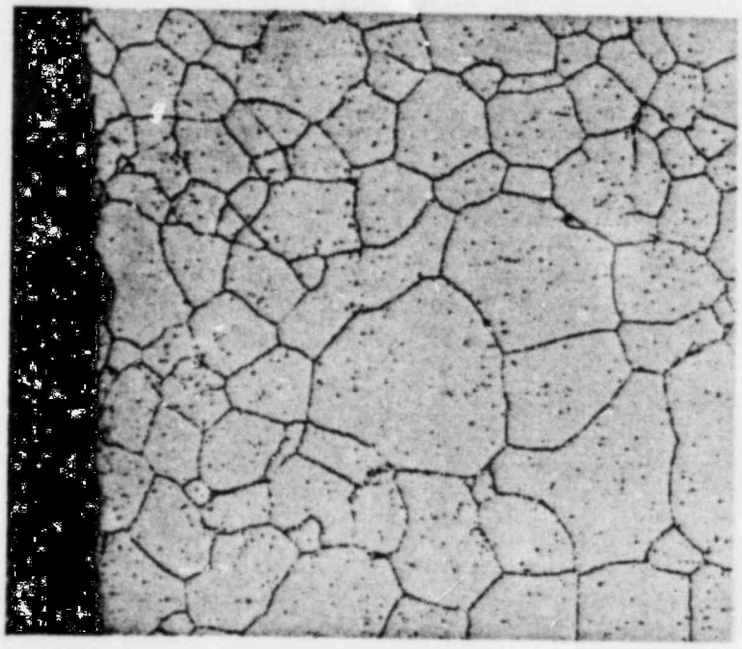

ID

500X H_3PO_4 Etch

(b) UNROLLED REGION

FIGURE 42. PHOTOMICROGRAPHS OF THE MICROSTRUCTURE OF TWO DIFFERENT REGIONS OF SPECIMEN B FROM TUBE A-146-8

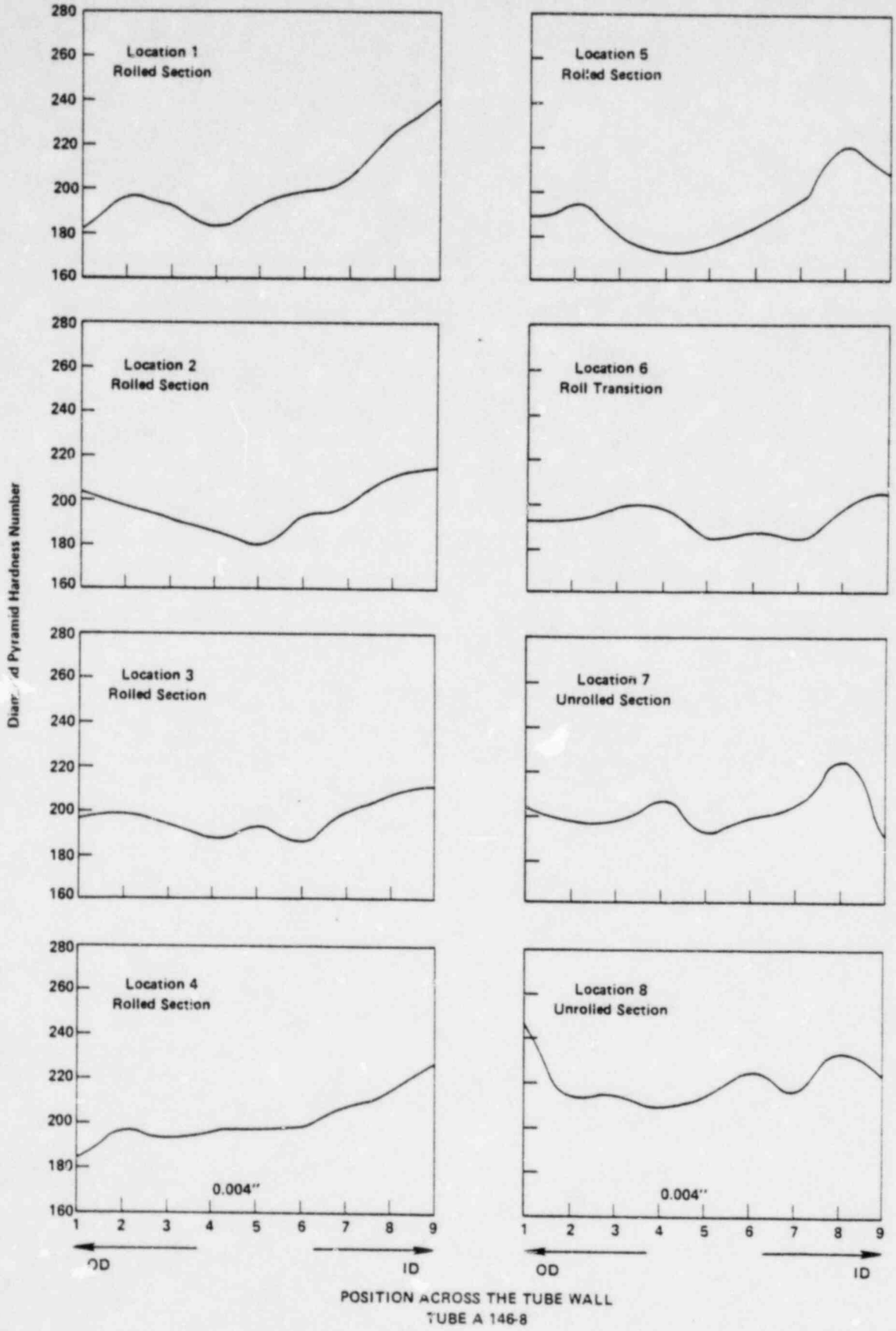

FIGURE 43. MICROHARDNESS VALUES AT 8 DIFFERENT SUB-LOCATIONS ON SPECIMEN B FROM TUBE A-146-8 (SEE TEXT)

The EPR sensitization test was done on specimen L from location 0.25-0.75 inch. The activation peak potential for this tube was 125 mV(SCE), which indicates a very high susceptibility to IGA by polythionic acid. This value is not significantly different from the 110 mV value obtained for other tubes.

A defect with EC indication at 3.75 inch was selected for SEM/EDAX and metallographic examinations. A circumferential crack at 3.75 inch location was visible to the unaided eyes. Some brown color decorations around the crack also were present. Two specimens containing the defect were prepared from location 3.5-4.5 inch, specimen E1 (90-180 degree) for metallographic examination, and specimen E2 (0-90 degree) for SEM/EDAX analysis.

The general appearance of the ID surface of the tube in the brown decoration area is shown in the SEM photograph in Figure 44. The surface is rough and is covered with granular and flaky deposits. Another spot from a similar area showed crusty deposits on the surface, as shown in the SEM photograph in Figure 45.

EDAX analysis of the spot in Figure 45 detected only Ni, Cr, Fe, Ti and S on the surface. The S was present in about 0.2 weight percent concentration. Approximate concentrations of other elements on the spot in atom percent were: Ni-44; Cr-25; Fe-20; and Ti-0.9. In relation to the composition of base metal, i.e., Inconel 600® the spot appears to be rich in Fe and Cr but depleted in Ni. Iron in the form of oxide may have produced the brown coloration on the surface.

The apparent crack in specimen E2 was mechanically pulled apart, and the fracture surface was examined in the SEM. A SEM photograph of the fractured surface in Figure 46 shows the intergranular nature of the crack. A photomicrograph of the same crack present in metallographic specimen E1 is shown in Figure 47. The crack is intergranular and penetration is ~70 percent through wall. No IGA was noticed on the ID or OD surface of the tube in the vicinity of the crack.

A transverse cross section of the tube, specimen F 3.5-4.25 inch, 180-360 degree, showed no IGA attack on the ID or OD when examined metallographically.

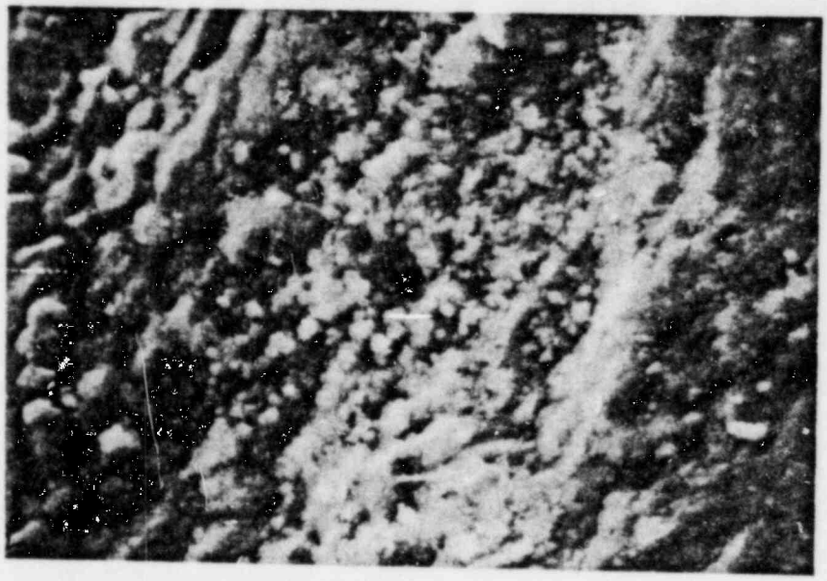

1300X

FIGURE 44. SEM PHOTOGRAPH OF A BROWN DECORATION ON THE ID SURFACE OF SPECIMEN E2 FROM TUBE A-146-8

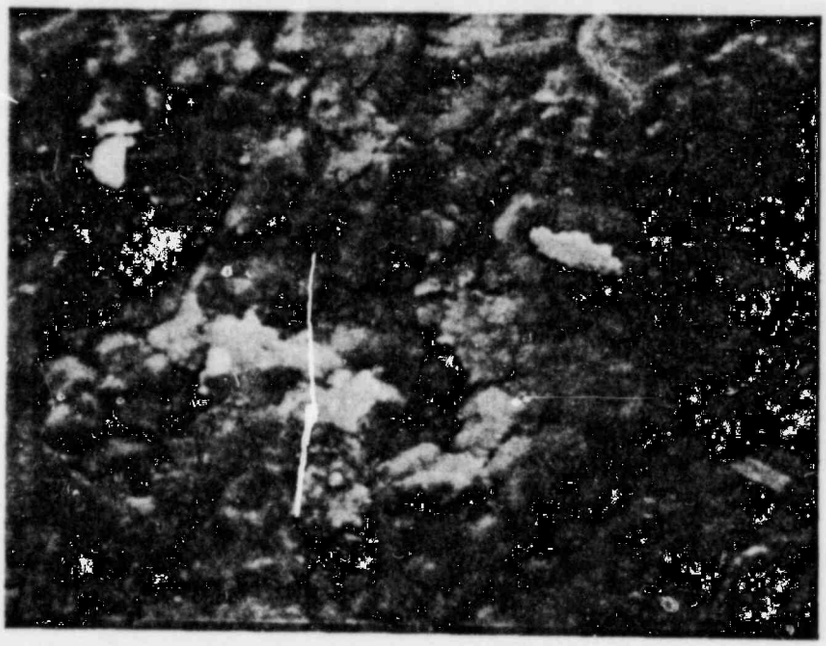

1300X

FIGURE 45. SEM PHOTOGRAPH OF A CRUSTY DEPOSIT IN A BROWN SPOT ON THE ID SURFACE OF SPECIMEN E1 FROM TUBE A-146-8

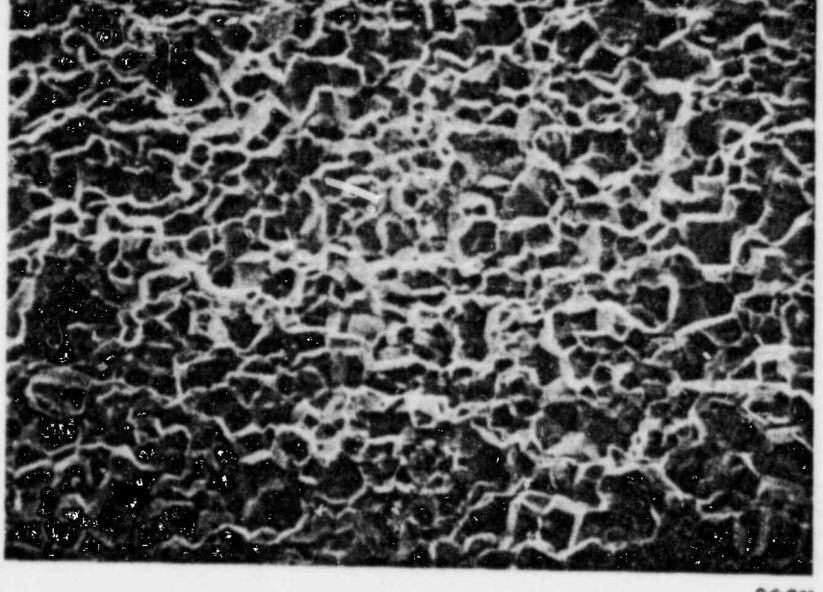

200X

FIGURE 46. SEM PHOTOGRAPH OF THE FRACTURE SURFACE OF SPECIMEN E2 FROM TUBE A-146-8

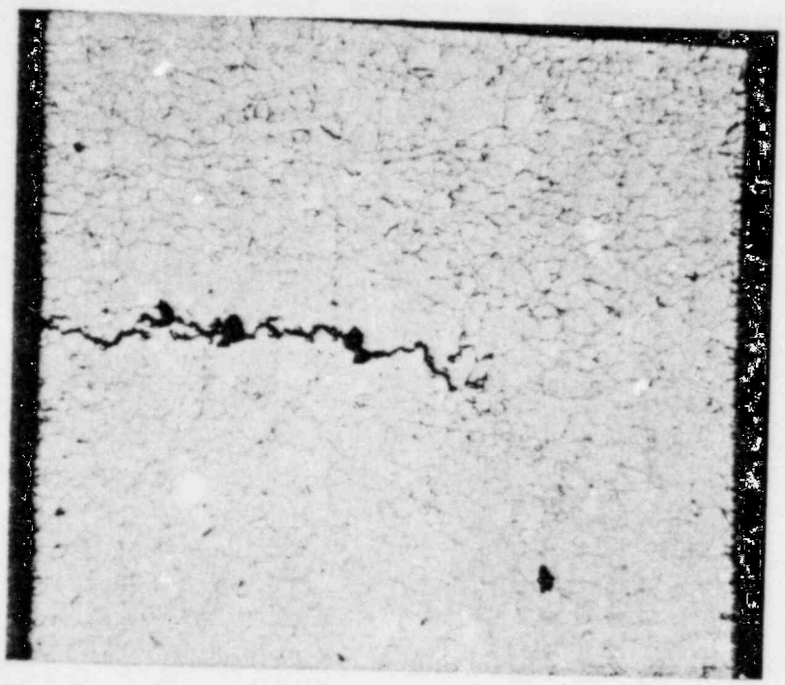

FIGURE 47. PHOTOMICROGRAPH OF AN IGC IN SPECIMEN E1 FROM TUBE A-146-8

Specimen I was taken from location 6.75-7.25 inch for another SEM and EDAX examination. There was no defect indication from NDE for this location, but a shallow pit was visible on the ID surface. A SEM photograph of the pit is shown in Figure 48. Encrustation around the pit is similar to that shown in Figure 45.

EDAX analysis of the surface found, in approximate atom percent, elements: Ni-44, Cr-41, Fe-12, Ti-0.8, S-0.8, and Si and Ca in small amounts. Another analysis of the inside surface of the pit found the deposits to be rich in Cr (76 percent) and low in Fe (~3 percent) and Ni (~17 percent). Other elements Ti, S, Ca and Si were also present in small amounts.

At one area inside the pit very high sulfur (7.8 percent) was detected, Ca (0.1 percent) and Ti (2.7 percent) also were present in the area. The descaled pit is shown in Figure 49. Intergranular attack is clearly visible in the SEM photograph.

Specimen G, location 8.5-9.0 inch, with no apparent defect on the ID surface and no NDE indication was examined metallographically. IGA was observed on the ID surface of the tube, as shown in Figure 50. The IGA is approximately 0.004 inch deep and 0.015 inch wide at the ID surface.

A lip-crack from location 0-0.5 inch was metallographically examined. Two specimens A and C from the 0-0.5 inch location were prepared for the examination. Specimen A, 0-180 degree, was examined in longitudinal cross section, whereas specimen C, 180-360 degrees, was examined in transverse cross section with respect to the tube axis.

Micrographs of specimens A and C are shown in Figures 51 and 52, respectively. In specimen A, the tube wall separated at the main crack while preparing the metallographic mount, the separated wall is visible in Figure 51. A second crack which appears to be a major branch of the main crack also is nearly through wall. The transverse section in specimen C showed three different unconnected cracks. One such crack only is shown in Figure 52; the other cracks were similar in nature.

Two specimens H and J from locations 8.5-9.0 inch and 10.5-11.0 inch showed no IGA attack on any surface ID or OD when examined metallographically. There were no NDE defect indication at the above locations.

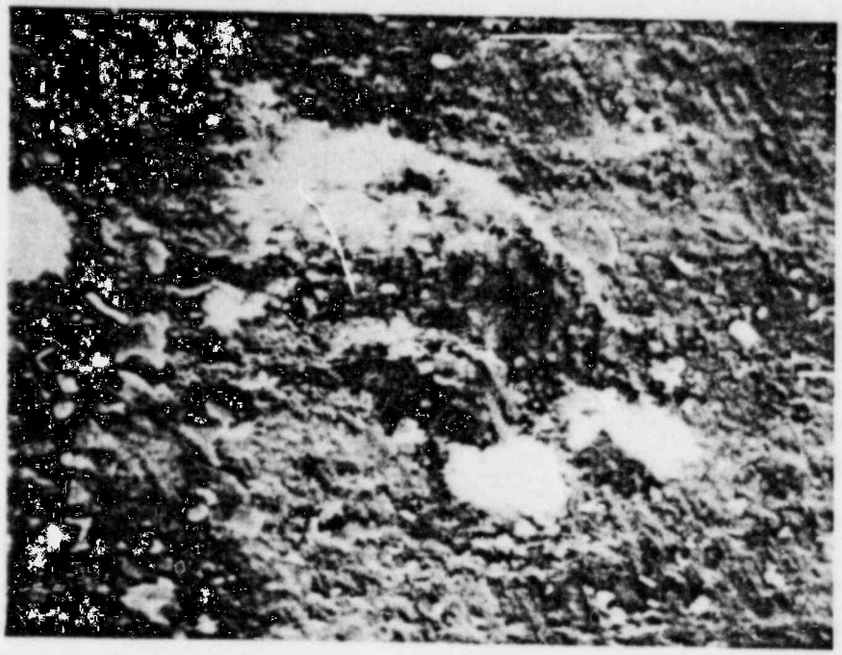

210X

FIGURE 48. SEM PHOTOGRAPH OF A SHALLOW PIT ON THE ID SURFACE OF SPECIMEN I FROM TUBE A-146-8

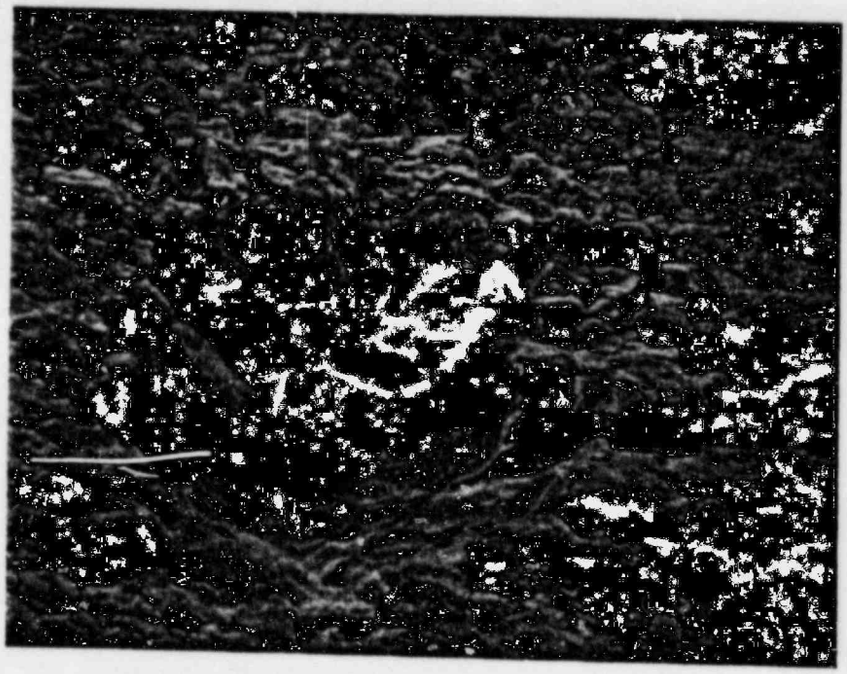

700X

FIGURE 49. SEM PHOTOGRAPH OF A DESCALED PIT ON THE ID SURFACE OF SPECIMEN I FROM THE TUBE A-146-8

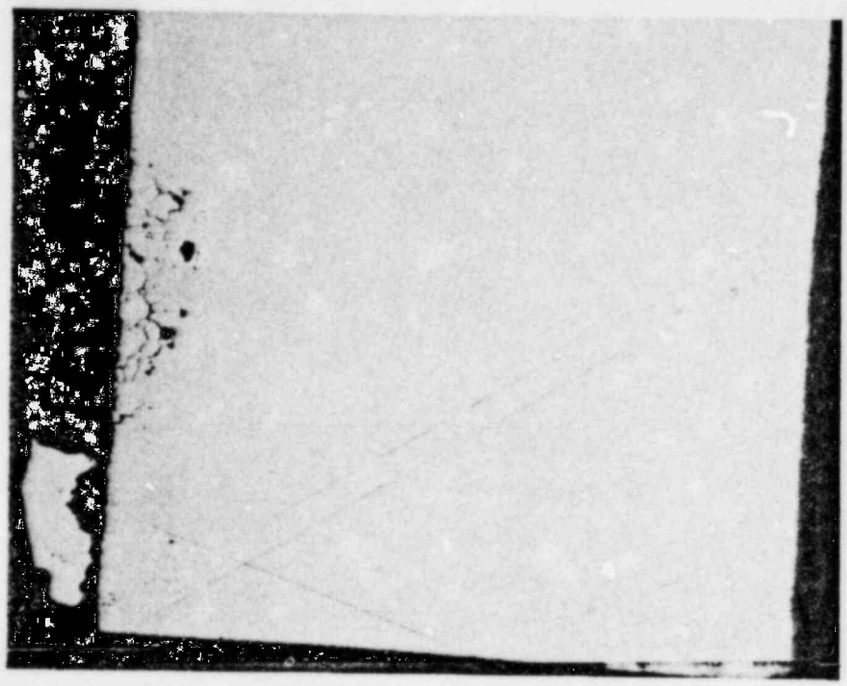

ID 100X OD

FIGURE 50. PHOTOMICROGRAPH OF AN IGA ON SPECIMEN G FROM TUBE A-146-8

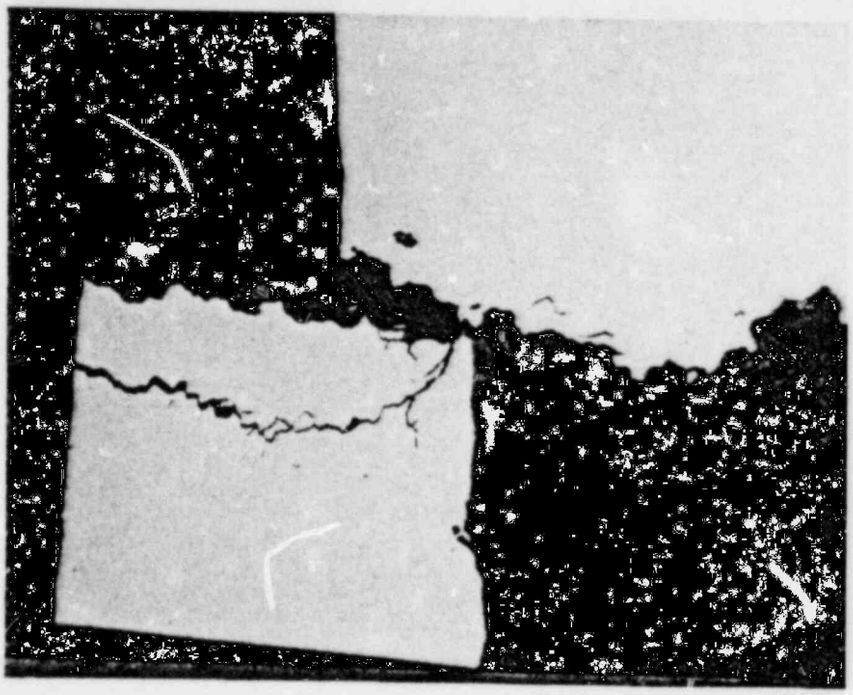

FIGURE 51. PHOTOMICROGRAPH OF AN IGC IN LONGITUDINAL CROSS SECTION OF SPECIMEN A FROM TUBE A-146-8

FIGURE 52. PHOTOMICROGRAPH OF AN IGC IN TRANSVERSE CROSS SECTION OF SPECIMEN C FROM TUBE A-146-8

Two more specimens, M and N, from locations 1.5-2.25 inch and 3.0-3.5 inch showed no defects on either the ID or OD surface in metallographic examinations. These specimens were particularly selected for OD examination since deposits were present on the OD surface. A similar result was obtained for tube A-146-6. It is reasonable to conclude that there are no defects on the OD side of tube A-146-6 or A-146-8.

5.0 RESULTS OF γ-RAY ISOTOPIC ANALYSIS

Five wipe samples from GPU-Nuclear were received for γ-ray isotopic analysis. Results of the analysis of each wipe sample are summarized in Table 27. Fission products detected on various samples were Am^{241}, Co^{57}, Sb^{125}, Ru^{106}, Ag^{110}, Cs^{134}, Mn^{54} and Co^{60}. The Co^{60} was the main source of γ-rays in these samples. The next most prevalent isotope was Ru^{106}. $Americium^{241}$ and Cs^{134} were detected on only one wipe sample which was from OTSG-B.

TABLE 27. GAMMA RAY ISOTOPIC ANALYSIS RESULTS

Isotope	ISOTOPE PERCENT SAMPLE IDENTIFICATION AU(1) R71T126 Sample #31	AU(2) R149T15 Sample #6	AL(3) Batch #66 Sample #20	BU(4) R75T3 Sample #13	BL(5) Batch #66 Sample #28
Am^{241}	--	--	--	--	0.1
Co^{57}	0.2	0.3	0.2	0.2	0.2
Sb^{125}	3.1	3.5	--	3.5	0.4
Ru^{106}	5.9	7.4	4.4	8.4	4.9
Ag^{110}	0.2	0.7	0.3	0.8	0.5
Cs^{134}	--	--	--	--	0.2
Mn^{54}	1.3	1.3	1.6	1.0	0.9
Co^{60}	89.3	86.8	93.5	86.1	92.8

Notes: (1) Whole sample analyzed; (2) ∿1/5th sample analyzed; (3) ∿1/5th sample analyzed;
(4) Whole sample analyzed; (5) ∿1/5th sample analyzed

6.0 DISCUSSION

The results of various examinations are discussed here. The aspects considered in the discussion are a) nature of defect, b) defect location vs. NDE, c) physical and chemical properties of OTSG tubes, d) surface film composition and finally, e) probable cause of attack.

Nature of Defects

Tubes A-146-6 and A-146-8 had typical dryout deposits on their OD surfaces. Four specimens, two from each tube, having these deposits, were metallographically examined in longitudinal and transverse cross section. The two specimens from tube A-146-6 were from just below the roll transition region, whereas those from tube A-146-8 were from the lower part of the tube segment. No IGA or other defects were observed on these specimens.

The OD surfaces of the above two tubes also were visually examined after brushing off the deposits at a few places. The surface underneath the deposit had a metallic luster, but no corrosion attack or significant etching was observed. The OD surfaces of these tubes were not examined in the SEM. However, on the basis of visual and metallographic results it is assumed that no OD defects exist under dryout deposits on tubes A-146-6 and A-146-8.

Since tubes A-146-6 and A-146-8 had typical dryout marks, it is likely that other tubes also do not have OD defects.

From the extensive metallurgical and SEM examinations of various specimens from different tubes, it is fairly obvious that the main mode of attack in the tubes is IGA. Further, the attack initiated on the ID surface of tubes. This attack produced three different kinds of defect geometry in the tube walls: a) IGA-islands, with grains retained, b) IGA-pits and, c) stress assisted deep intergranular penetrations which may be called intergranular stress corrosion cracks (IGSCC).

One prominent IGA island 0.004 inch deep and 0.015 inch wide on the ID surface of tube A-146-8 is shown in Figure 50. But some minor IGA areas were also seen in the SEM on a specimen from tube A-146-6. It is very likely that similar other islands are present on other tubes, particularly under ID deposits.

IGA-pits ranged in size from a few grains deep and a few grains wide, as in Figure 37 to ∿0.014 inch deep as in Figure 38. IGA-pits are a result of grain dropping from the heavily attacked IGA-islands. Grains from attacked areas dropped off either because the grain boundaries were heavily attacked and no cementing bond existed between the grains, or because of the force of voluminous corrosion products generated at the grain boundaries, or both. In some cases the voluminous corrosion product filled the entire pit; an example of this is in Figure 39.

The cracks, i.e., IGSCC, were circumferential and spanned from 1/8 to 3/4 of the circumference of a tube. The IGSCC penetration in various tube sections examined ranged between 20 and 100 percent through wall. Some of the cracks were wide open, e.g., in tube B-11-23, whereas others had to be opened up mechanically as in the case of B-8-25.

The IGSCC was produced in areas of IGA where stresses were high locally. A striking example of this is shown in Figure 38, in which the origin of the crack is clearly at the base of the pit. The pit in this case apparently had acted as a stress concentrator in the tube, and subsequently, high stresses opened the attack grain boundaries thus forming the crack.

Another example of IGA leading to IGSCC is the crack in tube B-11-23, Figure 25. The IGA was found three to four grains deep on the ID surface of the tube, ∿0.1 inch on either side of the main crack, Figure 26.

Most of the cracks examined had some branching. The IGA also was present along sides of crack walls, but the extent of IGA varied considerably from one crack to the next. Crack wall IGA was only one to two grains deep in some cases, see Figure 47, but seven to ten grains deep in others, Figure 25. Meandering of the crack or IGA in a plane perpendicular to the fracture surface is fairly evident in Figure 19. The deep cavities visible

in the mid wall are indicative of the spiraling. A similar conclusion can be drawn from Figure 52, which shows branched cracks present on a transverse section of tube A-146-8.

The three different kinds of defect geometries, mentioned earlier, mainly reflect different degrees of IGA at localized areas. Several factors related to mechanical, environmental and metallurgical conditions, e.g., localized stress, uneven distribution of aggressive chemicals (e.g., sulfur oxyanions and oxygen) on the tube surface, localized differences in degree of sensitization, uneven oxide film, surface deposits, inclusions, and manufacturing defects, etc., may have been responsible for the different geometries. Considerable amount of experimental work will be required to pin-point the actual cause.

There is, however, some indication in the literature* that the rate of IGA, in the case of polythionic acid corrosion of sensitized Type 304, is strongly stress dependent. The rate of IGA on sensitized Type 304 is substantially low in the absence of stress, but very high in the presence of applied stress. The actual rates were not given by the authors, but the unstressed specimens showed only minor IGA when they were exposed for 11 days in polythionic acid; on the other hand, the specimens stressed to 95 percent of their yield failed in a few hours.

If a similar condition is believed to apply to IGA in sensitized Inconel 600® tubes, the local variation in residual stresses could have been one principal cause of the different degree of attack observed in various parts of the same tube. But contributions from other factors, such as oxygen distribution, etc., cannot be completely ignored.

The possibility of tube failure due to corrosion fatigue was ruled out from the results of the TEM examination. No fatigue striations were observed on grain faces of the fracture examined, Figure 19.

Some mechanical defects also were found on the ID surface of several tubes. However, these were considered to be the results of either

---

* I. Matsushina, "Electrochemical Characteristics of Polythionic Acid Corrosion Cracking," Proceedings of the 6th International Congress on Metallic Corrosion, Sydney, Australia (1975).

the tube pulling operation or were manufacturing defects. The heavily scored ID surface of tube A-71-126 on metallographic examination showed mechanical indentations on the wall. The presence of deposits inside indentations suggest that the defects were caused by tube manufacturing processes and the deposits formed after the exposure of tubes to aqueous environment in the OTSG.

Physical and Chemical Properties of Tubes. The chemical composition, tensile properties, microhardness, grain size, and the microstructure with respect to carbide precipitates of tubes are those of a normal cold drawn stress relieved Inconel 600® tube. The grain size (ASTM No 7 - No. 8) was uniform at different locations examined for several tubes. No continuous network of carbides was observed in any tube, thus, indicating no severe sensitization. However, the EPR test showed that the tubes are in a heat treated condition which is very susceptible to polythionic acid intergranular attack. The EPR peak potentials of tubes were between 110 and 125 mV (SCE). During the EPR test, tubes were, in fact, heavily attacked intergranularly.

Surface Film Composition

The major foreign elements detected on the fracture surface of any specimen were C, S and Cl, not considering oxygen. The distribution of S on the surface was quite non-uniform, as shown by all the microanalytical techniques, i.e., EDAX, AES and ESCA. The concentration ranged from practically nothing (i.e., below detection limit) to almost 8 atom percent. Chlorine was detected only by ESCA at ∿1 atom percent level up to 2300 Å depth analyzed. Sulfur in the attacked area was found all the way down to the base metal as indicated by X-ray images of a shallow pit, see Figure 39. No chlorine was detected by this technique.

The concentration of carbon on the fracture surface was very high >50 atom percent and that of oxygen comparatively low, 18 atom percent.

Chemical states of the major elements were Ni as elemental Ni or tied to sulfur, Fe as FeO and Cr as Cr_2O_3. The S was in its reduced state as S^{-2}. The very low level of oxygen on the fracture surface agrees with the reduced states of Ni and S. Carbon was as in graphitic carbon or long-chain hydrocarbon.

Major constituents of the ID surface film on tube A-146-6 were Ni, Fe, Cr, O and C. Small amounts of B, S and Zr also were present. The same constituents also were found at location 52.0 inch on the long-pull tube A-71-126. Nominal concentrations of the elements as determined by ESCA up to a depth of 3500 Å on both tubes were (in atom percent) Ni 25, Fe 8, Cr 9, B 3, S 1, and Zr 0.2. No significant difference was observed in element concentrations because of the location of specimens with respect to the tube sheet. Sulfur was nominally at 1 atom percent. SIMS analysis of one specimen showed that S on the ID surface was persistent up to at least 1.5 μm depth.

The topmost layer (∿1100 Å) of the ID surface film was somewhat oxidized (e.g., S as $SO_4^{=}$; Ni as NiO) as indicated by ESCA. But thereafter, reduced S as $S^{=}$ was the prevalent form. Nickel, Fe and Cr at this level were as Ni and NiO, FeO and Cr_2O_3.

These analyses show that there is no significant difference between the states of elements on the fracture surface and the lower layers of the ID surface. The one noticeable difference is that C on the fracture surface is at twice the concentration of that on the ID surface. The oxygen level is also two to three times higher on the ID surface, but this could be simply because the ID surface was exposed to ambient environment for a long time, whereas the IGA-affected areas were protected by corrosion products.

The presence of high carbon in the ID surface film and in the fractured surface film is disconcerting. The SIMS analysis of ID surface, Figure 40, showed that C is persistent down to ∿2.0 μm depth analyzed. The fracture surface film was analyzed with AES/ESCA to only ∿2300 Å (0.23 μm) depth, but it is likely that C was present at greater depths. In both cases, the chemical form of C determined by ESCA was the same,

the binding energy for C atoms was as in graphitic-carbon or long chain hydrocarbons. It is reasonable to conclude that the C was deposited on both the surfaces from the same source.

The tube specimens for surface analyses was sectioned using a hand operated jeweler's saw (hack saw). No lubricants were used in the operation. Sectioned specimens were stored immediately in clear plastic vials. The possibility of specimen contamination with carbon during sectioning and handling operations was therefore low.

However, minor contamination of specimens from air exposure and also inside the vacuum chamber (from residual vacuum pump oil vapors) of instruments is a definite possibility. Carbon from such contamination is often detected on specimens in AES/ESCA analyses. But this type of contamination is usually limited to the uppermost layer (50 to 100 Å) of the surface film on specimens, if the film is non-porous. The contamination is easily removed by argon ion sputtering.

During the AES/ESCA analyses of OTSG tubes, the specimen holder, which was made of copper, was checked in a few instances for surface contamination. Carbon was detected on the copper holder prior to any argon ion sputtering, but after about 50 Å of sputtering, C was virtually all removed.

In the case of specimens with porous surface film, which probably was the case with OTSG tubes, the C contamination could have been deeper, and therefore, not easily cleaned off by argon ion sputtering. It is likely, therefore, that the total C measured on the tube surfaces had some contribution from contamination in the instrument. The exact contribution to C analyzed is not determinable, but it is considered to be a small fraction of the total.

The Preliminary Failure Analysis Report issued by GPU-N indicates that some oil may have been accidently introduced in the reactor coolant during the plant layup in March, 1979. It is likely that some oil migrated to the steam generators, adhered on the tube walls and permeated the surface film. The chemical form of C in the oil would easily account for that determined by ESCA on various tube specimens.

If the oil was not removed from the OTSG system, it is likely that the oil survived the hot functional and it was present in the system during the subsequent layup. If the cracking of tubes occurred (either before or after the hot functional) when the oil was present in the system, indeed carbon could have deposited on the fracture surfaces. The fracture surfaces (Figure 21) analyzed by AES/ESCA were from a crack which had penetrated ~90 percent of the tube wall. Therefore, it can be presumed that the crack walls were sufficiently open, under the tensile stress present during the cold layup, to allow entry of oil into the crack.

Defect Location vs NDE

Defects confirmed by destructive examination of numerous specimens from different tubes always corresponded to EC observations, except in two cases. In tube A-146-6 at location 6.0 inch, a small pit was observed, Figure 39, which was not detected by EC at Battelle, and the GPU-Nuclear EC data file also does not show any indication for this position. Similarly, no EC indications were given by either Battelle or GPU-Nuclear for the IGA defect, Figure 50, in tube A-146-8 at location 8.75 inch.

The first undetected defect, i.e., the pit was rather small, 0.003 inch in diameter and 0.001 inch deep, but the IGA was 10 percent through wall. Sizes of the above defects are almost below the detection limit of some of the EC probes.

Defect indications obtained from radiographs were not always confirmed as IGSCC or IGA. These indications were most probably from the scoring of ID surface during tube pulling operation. Radiographs also were not able to detect very tight cracks.

A majority of confirmed defects in tubes were located in the roll transition area. The main reason for the preponderance of cracks in that area appears to be high concentration of stress, which assisted in propagation of IGA as discussed earlier.

Probable Cause of Attack and Failure Scenario

Considerable amount of sulfur was detected on the ID surface of tubes, inside pits, and on fracture surfaces. Sodium thiosulfate and sulfuric acid were accidently introduced several times into the reactor cooling system between 1980 and 1981 during the plant layup. Undoubtedly, these were the source of sulfur on the tubes. Sulfur compounds, such as thiosulfate and polythionic acids are known* to produce IGSCC in sensitized Inconel 600® alloy in the presence of oxygen in the environment. The heat treatment of tubes was such that they were extremely susceptible to IGSCC by polythionic acid, as indicated by the EPR results. Therefore, the most probable cause of IGA on the OTSG tubes appear to be sulfur compounds.

The exact period in which the attack occurred, between 1980 and the time when the defects in tubes were first suspected, is uncertain. The OTSGs were brought to hot-functional status in August-September, 1981, and at this time no leaks were detected nor any defects were suspected. Leaks in tubes were detected the first time during the hydrotest in November, 1981, and subsequent EC examination indicated defects in a large number of tubes in both OTSGs A and B. The absence of any leak during the hot-functional operation strongly suggests that the defects in the tubes developed mostly afterwards.

The sequence of events leading to post hot-functional IGA of tubes is postulated to be as follows: (1) The environment inside the OTSGs during the layup period prior to hot-functional was devoid of oxygen but contaminated with sulfur compounds (i.e., thiosulfate and H_2SO_4). Any trace amount of oxygen in the system, if present at all, was probably consumed by some of the thiosulfate (say, $Na_2S_2O_3 + H_2O + O_2 = Na_2SO_4 + H_2SO_4$). Because of the absence of oxygen, the Inconel 600® tubes did not suffer the IGA to any significant extent during this period. (2) The sulfur detected on

---

* Karl Sieradzki, et al., Paper No. 224, Corrosion/82, Houston (1982)

on the tubes is primarily in the form of sulfide (NiS or Ni_2S_3). The sulfur compounds present in the OTSGs were reduced to either sulfur or sulfide at high temperature in the presence of hydrogen during the hot-functional. The reduced compounds ultimately reacted with the tube surface producing the sulfide film. (3) Following the hot-functional, the OTSGs were partly drained for plant maintenance. The water level was kept near the upper tube sheet, but fluctuated by several inches between September and November of 1981. The atmosphere inside the channel head during this period was primarily air. It is believed that the nickel sulfide reacted with the oxygenated water and produced the polythionic acid (e.g., $8NiS + 2H_2O + 11O_2 = 4Ni_2O_3 + 2H_2S_4O_6$), by a mechanism similar to that proposed originally by Brophy* and later confirmed by Ahmad et al.* The polythionic acid attacked the susceptible Inconel 600® and produced the IGA.

The attack was primarily limited to those regions of tubes where the stress concentration was high and the oxygen was readily available. The above two conditions were adequately present at the water/air interface in the upper tube sheet region, particularly at the rolled section of tubes. This explains the preponderance of defects in tubes in the upper tube sheet region. (4) Several elements, primarily fission products and carbon, beside sulfur were detected on the tube surface as well as on fracture surfaces. Whether these elements played any role in the attack mechanism can not be said with certainty. However, in view of the strong attack by polythionic acid, the role of other elements is considered to be nominal, if any.

---

* S. Ahmad et al., Corrosion. 38, 347 (1982).

7.0 CONCLUSIONS

Our general conclusions regarding the failure of Inconel 600® tubes in the OTSC A and B of TMI-1, based on examination results are as follows:

(1) Inconel 600® tubes failed by intergranular cracking (IGC)

(2) The cracks initiated on the inside surface of tubes and propagated outward.

(3) The cracks are characterized by severe intergranular attack (IGA) on either side of the crack

(4) Some small areas on the inside surface have IGA ∿ 5 mils deep but with no cracks associated with them.

(5) The cracks and the IGA have been found in the entire length of the short-pull section of tubes.

(6) Whether the attack (IGA or IGC) extends beyond the short-pull length has not been fully evaluated

(7) There was a preponderance of cracks in the roll transition region of tubes, high stress concentration in that part of the OTSG appears to be responsible

(8) The most probable species responsible for the intergranular attack are the derivatives of sulfur (such as polythionic acid and thiosulfate) which was found in significant concentration on the fracture surface

(9) There was no defect observed on the OD side of tubes under dryout deposits

(10) Some fission products, carbon and beryllium also were found on the fracture surface and on the inside surface of tubes; their role, if any, on the tube degradation process(es) is not discernible at present.

(11) The attack on tubes most probably occurred during the layup following the hot-functional.

8.0 ACKNOWLEDGMENTS

The following persons actively participated in accomplishing the work cited herein. Paul Tomlin with metallography and radiography; A. E. Austin with Auger, ESCA and secondary ion mass spectroscopy; Gene Sands with scanning electronmicroscopy and energy dispersive X-ray analysis; Don Hayford with eddy current examination; Larry Lowry with γ-ray analysis and tensile testing; and Andy Skidmore with TEM. The arduous task of typing this report in a hurry was done by Irene Knight.